Journal of the Mechanics and Physics of Solids 58 (2010) 1963–1994

Contents lists available at ScienceDirect

Journal of the Mechanics and Physics of Solids

journal homepage: www.elsevier.com/locate/jmps

Size effects in generalised continuum crystal plasticity for two-phase laminates

N.M. Cordero [a], A. Gaubert [b], S. Forest [a,*], E.P. Busso [a], F. Gallerneau [b], S. Kruch [b]

[a] MINES ParisTech, Centre des matériaux, CNRS UMR 7633, BP 87, 91003 Evry Cedex, France
[b] Department of Metallic Materials and Structures, ONERA, 29, Avenue de la Division Leclerc, 92322 Chatillon Cedex, France

ARTICLE INFO

Article history:
Received 19 October 2009
Received in revised form
22 June 2010
Accepted 25 June 2010

Keywords:
Crystal plasticity
Strain gradient plasticity
Cosserat medium
Micromorphic theory
Dislocation density tensor

ABSTRACT

The solutions of a boundary value problem are explored for various classes of generalised crystal plasticity models including Cosserat, strain gradient and micromorphic crystal plasticity. The considered microstructure consists of a two-phase laminate containing a purely elastic and an elasto-plastic phase undergoing single or double slip. The local distributions of plastic slip, lattice rotation and stresses are derived when the microstructure is subjected to simple shear. The arising size effects are characterised by the overall extra back stress component resulting from the action of higher order stresses, a characteristic length l_c describing the size-dependent domain of material response, and by the corresponding scaling law l^n as a function of microstructural length scale, l. Explicit relations for these quantities are derived and compared for the different models. The conditions at the interface between the elastic and elasto-plastic phases are shown to play a major role in the solution. A range of material parameters is shown to exist for which the Cosserat and micromorphic approaches exhibit the same behaviour. The models display in general significantly different asymptotic regimes for small microstructural length scales. Scaling power laws with the exponent continuously ranging from 0 to -2 are obtained depending on the values of the material parameters. The unusual exponent value -2 is obtained for the strain gradient plasticity model, denoted "$curl\,H^p$" in this work. These results provide guidelines for the identification of higher order material parameters of crystal plasticity models from experimental data, such as precipitate size effects in precipitate strengthened alloys.

1. Introduction

Classical continuum crystal plasticity theory incorporates internal variables associated with scalar dislocations densities in order to describe the hardening behaviour of single crystals and polycrystals (McDowell, 2008). The modelling of size effects observed in crystalline solids, such as grain or precipitate size effects, has been addressed by adding strain gradient variables into the constitutive framework, either in an explicit way as in Acharya and Beaudoin (2000), Busso et al. (2000) and Bassani (2001) or by means of additional degrees of freedom associated with new boundary and interface conditions (Forest et al., 1997; Shu, 1998). Motivations for introducing strain gradients in continuum modelling stem from the multiscale analysis of micromechanics, as reviewed in Ghoniem et al. (2003). The resulting strain gradient components are related to the dislocation density tensor as introduced by Nye (1953). The dislocation density tensor is computed from

* Corresponding author. Tel.: +33 1 60 76 30 51; fax: +33 1 60 76 31 50.
E-mail address: Samuel.Forest@ensmp.fr (S. Forest).

0022-5096/$ - see front matter © 2010 Elsevier Ltd. All rights reserved.
doi:10.1016/j.jmps.2010.06.012

the rotational part of the gradient of plastic deformation, so that the partial differential equations to be solved generally are of higher order than those used in classical mechanics. That is why it is usually necessary to resort to the mechanics of generalised continua in order to properly formulate models that incorporate extra-hardening effects associated with the dislocation density tensor. Generalised crystal plasticity models developed in the past forty years can be classified into two main groups:

- Strain gradient plasticity models involving either the rotational part of plastic deformation or its full gradient (Aifantis, 1984, 1987; Steinmann, 1996; Fleck and Hutchinson, 1997; Gurtin, 2002; Cheong et al., 2005; Lele and Anand, 2008),
- Generalised continuum theories with additional degrees of freedom accounting for rotation or full deformation of a triad of crystal directors and the effect of their gradients on hardening: Cosserat models (Kröner, 1963; Forest et al., 2000; Clayton et al., 2006), and models based on micromorphic theory (Eringen and Claus, 1970; Bammann, 2001).

Most of these phenomenological theories have been shown to capture size effects at least in a qualitative way. However, clear demonstrations that they can reproduce the scaling laws expected in precipitate hardening or grain size effect, namely Orowan and Hall-Petch laws, have not been yet provided.

The extra-hardening effects predicted by generalised continuum crystal plasticity models can be summarised in the main features identified in Fig. 1, which shows schematically in a log–log diagram the effect of the microstructural length scale l (grain or precipitate size) on flow stress. These three main characteristics are the stress range, $\Delta\Sigma$, the characteristic length, l_c, and the scaling law, $\Sigma \propto l^n$ when $l \approx l_c$. Here, $\Delta\Sigma$ also corresponds to the highest overstress reached for small microstructural length scales, that is why $\Delta\Sigma$ is also called the extra-stress in this work. Fig. 1 shows that when the characteristic size of the microstructure decreases, the material strengthens. For large values of l, the asymptotic behaviour corresponds to the size-independent response of conventional crystal plasticity models. In contrast, for small values of l, a bounded or unbounded asymptotic behaviour can be obtained, depending on the model considered. The Cosserat crystal plasticity model proposed by Forest et al. (2000), for instance, predicts an asymptotically saturated extra-stress $\Delta\Sigma$ (see Fig. 1). In the intermediate region around the characteristic length l_c, the size-dependent response can be characterised by the scaling law, $\Sigma \propto l^n$, in the proximity of $l=l_c$. The objective of the present work is to derive explicitly the characteristics $\Delta\Sigma$, l_c and n, for models representative of the above classes of generalised material models.

An analytic description of the size-dependent behaviour of materials is possible only in some special simplified geometrical situations. For instance the prediction of the shearing of a single crystal layer under single (or double) slip for strain gradient plasticity models was treated in Shu et al. (2001), Bittencourt et al. (2003), Bardella (2007) and Hunter and Koslowski (2008). Single slip in a two-phase laminate microstructure was considered in Sedláček and Forest (2000), Forest and Sedláček (2003) and Forest (2008). Here, the plastic slip distributions were compared with those obtained from the continuous dislocation line tension model, considered as a reference, and Cosserat and strain gradient plasticity models, including that proposed by Aifantis (1987). This simple situation is considered again in the present work in order to derive explicit expressions for the overall extra-hardening, the characteristic length scale l_c and the Σ–l scaling law, which had not been done in the previous work.

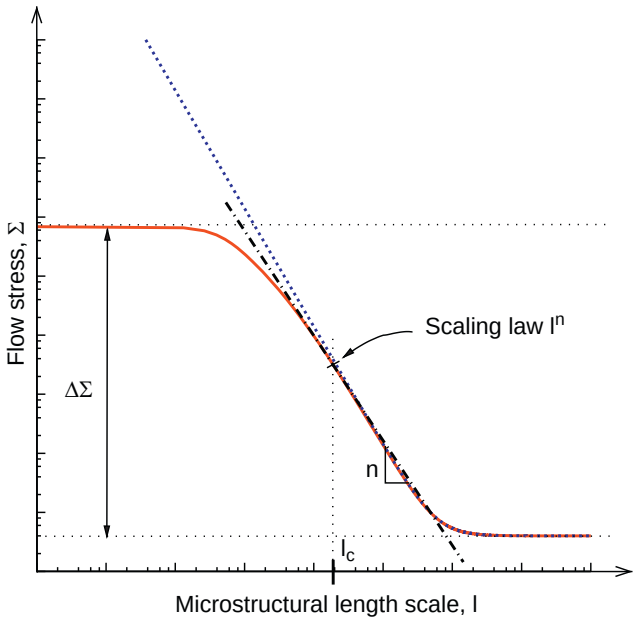

Fig. 1. Description of two different profiles of the macroscopic flow stress that can be obtained with the different groups of models: size effect with two asymptotic regimes (solid line), unbounded extra-stress for small sizes (dotted line), definition of the scaling law in the transition domain (dot-dashed line).

In the crystal plasticity theory at small deformation, the gradient of the velocity field can be decomposed into the elastic and plastic deformation rates:

$$\dot{\underset{\sim}{\boldsymbol{H}}} = \dot{\underline{\boldsymbol{u}}} \otimes \boldsymbol{\nabla} = \dot{\underset{\sim}{\boldsymbol{H}}}^{e} + \dot{\underset{\sim}{\boldsymbol{H}}}^{p}, \tag{1}$$

where

$$\dot{\underset{\sim}{\boldsymbol{H}}}^{p} = \sum_{\alpha} \dot{\gamma}^{\alpha} \underline{\boldsymbol{l}}^{\alpha} \otimes \underline{\boldsymbol{n}}^{\alpha}, \tag{2}$$

with $\underline{\boldsymbol{u}}$ the displacement field, α the number of slip systems, $\dot{\gamma}^{\alpha}$ the slip rate for the slip system α, $\underline{\boldsymbol{l}}$ the slip direction and $\underline{\boldsymbol{n}}$ the normal to the slip plane. The elastic deformation $\underset{\sim}{\boldsymbol{H}}^{e}$ bridges the gap between the compatible total deformation $\underset{\sim}{\boldsymbol{H}}$ and the incompatible plastic deformation $\underset{\sim}{\boldsymbol{H}}^{p}$. Applying the curl operator to a compatible field gives zero so that

$$\operatorname{curl} \dot{\underset{\sim}{\boldsymbol{H}}} = 0 = \operatorname{curl} \dot{\underset{\sim}{\boldsymbol{H}}}^{e} + \operatorname{curl} \dot{\underset{\sim}{\boldsymbol{H}}}^{p}. \tag{3}$$

The incompatibility of plastic deformation is characterised by its curl part called dislocation density tensor $\underset{\sim}{\boldsymbol{\Gamma}}$ (Nye, 1953; Steinmann, 1996; Forest et al., 1997; Acharya and Bassani, 2000; Cermelli and Gurtin, 2001; Svendsen, 2002) defined here as

$$\underset{\sim}{\boldsymbol{\Gamma}} = -\operatorname{curl} \underset{\sim}{\boldsymbol{H}}^{p} = \operatorname{curl} \underset{\sim}{\boldsymbol{H}}^{e}. \tag{4}$$

The tensors $\underset{\sim}{\boldsymbol{H}}, \underset{\sim}{\boldsymbol{H}}^{e}, \underset{\sim}{\boldsymbol{H}}^{p}$, generally non-symmetric, can be decomposed into their symmetric and skew-symmetric parts:

$$\underset{\sim}{\boldsymbol{H}} = \underset{\sim}{\boldsymbol{\varepsilon}} + \underset{\sim}{\boldsymbol{\omega}}, \quad \underset{\sim}{\boldsymbol{H}}^{e} = \underset{\sim}{\boldsymbol{\varepsilon}}^{e} + \underset{\sim}{\boldsymbol{\omega}}^{e}, \quad \underset{\sim}{\boldsymbol{H}}^{p} = \underset{\sim}{\boldsymbol{\varepsilon}}^{p} + \underset{\sim}{\boldsymbol{\omega}}^{p}. \tag{5}$$

Then Eq. (3) becomes

$$0 = \operatorname{curl} \underset{\sim}{\boldsymbol{\varepsilon}}^{e} + \operatorname{curl} \underset{\sim}{\boldsymbol{\omega}}^{e} + \operatorname{curl} \underset{\sim}{\boldsymbol{H}}^{p}. \tag{6}$$

Neglecting the curl part of the elastic strain, $\underset{\sim}{\boldsymbol{\varepsilon}}^{e}$, leads to the following approximation to the dislocation density tensor derived by Nye:

$$\underset{\sim}{\boldsymbol{\Gamma}} = \operatorname{curl} \underset{\sim}{\boldsymbol{H}}^{e} = \operatorname{curl} \underset{\sim}{\boldsymbol{\varepsilon}}^{e} + \operatorname{curl} \underset{\sim}{\boldsymbol{\omega}}^{e} \simeq \operatorname{curl} \underset{\sim}{\boldsymbol{\omega}}^{e}. \tag{7}$$

Nye's formula sets a linear relationship between this approximation of the dislocation density tensor and lattice curvature. The Cosserat crystal plasticity theory developed in Forest et al. (1997) incorporates the effect of lattice curvature on crystal hardening behaviour. It requires three additional degrees of freedom associated with the lattice rotation $\underset{\sim}{\boldsymbol{\omega}}^{e}$. In contrast, the theories proposed by Gurtin (2002) and Svendsen (2002), for example, include the full curl of the plastic deformation. This requires in general nine additional degrees of freedom associated with the generally non-symmetric plastic deformation tensor $\underset{\sim}{\boldsymbol{H}}^{p}$. We will call this sub-class of models "$curl\, H^{p}$" .

A consequence of neglecting the curl of elastic strain tensor in the Cosserat model is that Cosserat effects can arise even in the elastic regime as soon as a gradient of "elastic" rotation exists. Indeed, the $\operatorname{curl} \underset{\sim}{\boldsymbol{\omega}}^{e} \neq 0$ as soon as $\operatorname{curl} \underset{\sim}{\boldsymbol{\varepsilon}}^{e} \neq 0$. In contrast, in the $curl\, H^{p}$ theory, strain gradient effects arise only when plastic deformation has developed. As it will be shown in this work, this leads to different predicted behaviour at the interface between an elastic and a plastic phase.

The work presented there is organised as follows. Strain/stress fields and the back stress in a laminate microstructure, made of a hard elastic and a soft plastic phase, submitted to simple shear are derived for the Cosserat theory in Section 2 and for a "$curl\, H^{p}$" type model in Section 3. It will be shown that a jump in the generalized tractions arises at the interface according to the latter approach, due to the presence of a purely elastic phase. A regularisation method is proposed in Section 4 by introducing a model, called *microcurl*, that falls into the class of generalised continua with additional degrees of freedom. A comparison of the size effects predicted by the Cosserat and *microcurl* models is presented in Section 5. In Section 6, we discuss how our results could be used to identify strain gradient plasticity parameters from experimentally observed size effects, such as precipitate size effects in two-phase single crystal nickel based superalloys published by Busso et al. (2000), Forest et al. (2000) and Tinga et al. (2008). The solution is finally extended to the case of symmetric double slip. It is shown that very similar size effects as those for the single slip case are found, opening the way to further multislip generalisations of the models. The notation used hereafter is given in Appendix A.

2. Cosserat modelling of simple shear in a two-phase laminate

Simple shear of a two-phase laminate was considered first in Sedláček and Forest (2000) and then explored in more details in Forest and Sedláček (2003) and Forest (2008) from the point of view of the continuum theory of dislocations, on the one hand, and for Cosserat and strain gradient continuum plasticity models, on the other hand. Analytic solutions of the boundary value problem were derived for the stress, strain and plastic slip profiles in the microstructure. According to the Cosserat model presented in Forest (2008), a back stress intrinsically arises from the skew symmetric contribution

of the stress and orientation tensors, when writing Schmid law. The objective of this section is to recall the main features of the Cosserat approach, and to derive the main characteristics of the size effect, given by the maximum stress amplitude, $\Delta\Sigma$, the characteristic length scale of the transition zone, l_c, and the scaling law exponent, n.

2.1. The Cosserat formulation

A Cosserat continuum is described by a displacement field $\underline{\boldsymbol{u}}$ and an independent micro-rotation field, represented by its axial vector, $\underline{\boldsymbol{\phi}}$. Two deformation measures are then defined:

$$\underset{\sim}{\boldsymbol{e}} = \underline{\boldsymbol{u}} \otimes \boldsymbol{\nabla} + \underset{\sim}{\boldsymbol{\epsilon}} \cdot \underline{\boldsymbol{\phi}}, \quad e_{ij} = u_{i,j} + \epsilon_{ijk}\phi_k, \tag{8}$$

$$\underset{\sim}{\boldsymbol{\kappa}} = \underline{\boldsymbol{\phi}} \otimes \boldsymbol{\nabla}, \quad \kappa_{ij} = \phi_{i,j}, \tag{9}$$

where $\underset{\sim}{\boldsymbol{e}}$ represents the relative deformation tensor and $\underset{\sim}{\boldsymbol{\kappa}}$ the curvature tensor. The stress tensors associated with the previous deformation and curvature are the force stress tensor, $\underset{\sim}{\boldsymbol{\sigma}}$, and the couple stress tensor, $\underset{\sim}{\boldsymbol{m}}$. Both have to fulfil the balance of momentum and balance of moment of momentum equations:

$$\operatorname{div} \underset{\sim}{\boldsymbol{\sigma}} = 0, \quad \sigma_{ij,k} = 0, \tag{10}$$

$$\operatorname{div} \underset{\sim}{\boldsymbol{m}} + 2\overset{\times}{\underline{\boldsymbol{\sigma}}} = 0, \quad m_{ij,j} - \epsilon_{ijk}\sigma_{jk} = 0. \tag{11}$$

Note that volume forces and couples are not considered for simplicity. In Eq. (11), $\overset{\times}{\underline{\boldsymbol{\sigma}}}$ is the axial vector associated with the skew-symmetric part of the stress tensor,

$$\overset{\times}{\underline{\boldsymbol{\sigma}}} = -\frac{1}{2}\underset{\sim}{\boldsymbol{\epsilon}} : \underset{\sim}{\boldsymbol{\sigma}}. \tag{12}$$

Moreover, the boundary conditions for the traction and couple stress vectors are

$$\underline{\boldsymbol{t}} = \underset{\sim}{\boldsymbol{\sigma}}.\underline{\boldsymbol{n}}, \quad t_i = \sigma_{ij}n_j, \tag{13}$$

$$\underline{\boldsymbol{m}} = \underset{\sim}{\boldsymbol{m}}.\underline{\boldsymbol{n}}, \quad m_i = m_{ij}n_j, \tag{14}$$

where $\underline{\boldsymbol{n}}$ is the unit normal vector to the boundary of the considered domain. The deformation can be decomposed into its elastic and plastic parts,

$$\underset{\sim}{\boldsymbol{e}} = \underset{\sim}{\boldsymbol{e}}^e + \underset{\sim}{\boldsymbol{H}}^p. \tag{15}$$

Plastic deformation is due to slip processes and the evolution of $\underset{\sim}{\boldsymbol{H}}^p$ is still given by Eq. (2). The constitutive equations for isotropic Cosserat elasticity can be expressed as

$$\underset{\sim}{\boldsymbol{\sigma}} = \lambda(\operatorname{tr} \underset{\sim}{\boldsymbol{e}}^e)\underset{\sim}{\mathbf{1}} + 2\mu\underset{\sim}{\boldsymbol{e}}^{es} + 2\mu_c\underset{\sim}{\boldsymbol{e}}^{ea}, \tag{16}$$

$$\underset{\sim}{\boldsymbol{m}} = \alpha(\operatorname{tr} \underset{\sim}{\boldsymbol{\kappa}})\underset{\sim}{\mathbf{1}} + 2\beta\underset{\sim}{\boldsymbol{\kappa}}^s + 2\gamma\underset{\sim}{\boldsymbol{\kappa}}^a, \tag{17}$$

where λ and μ are the classical Lamé constants, and μ_c, α, β and γ are four additional elastic constants. In a 2D situation, as it is the case in this work, the constant α is not relevant and we choose $\beta = \gamma$ for simplicity. The size effects exhibited by the solutions of boundary value problems involving such a model are related to an intrinsic length scale, typically defined as

$$l_\omega = \sqrt{\frac{\beta}{\mu}}. \tag{18}$$

In the present work, the constraint

$$\mu/\mu_c \ll 1 \tag{19}$$

is enforced. This condition implies that $\underset{\sim}{\boldsymbol{e}}^e$ is almost symmetric and therefore means that the Cosserat micro-rotation almost coincides with the lattice rotation. The parameter μ_c can be seen as a penalty factor that constrains the Cosserat directors to be lattice vectors (Forest et al., 2001). The curvature tensor $\underset{\sim}{\boldsymbol{\kappa}}$ is then directly related to the curl $\underset{\sim}{\boldsymbol{\omega}}^e$ through Nye's formula (Forest, 2008). It follows that the curvature tensor of the Cosserat theory stands as an approximation to the dislocation density tensor.

Here the Schmid criterion is used as the yield criterion, computed with the generally non-symmetric force stress tensor. Furthermore, the critical resolved shear stress, τ_c, is taken to be constant for the analytic developments of this work (thus no strain-hardening is considered). The generalised resolved shear stress for the slip system α, defined by its slip plane normal vector $\underline{\boldsymbol{n}}^\alpha$, and its slip direction vector $\underline{\boldsymbol{l}}^\alpha$, is obtained from

$$\tau^\alpha = \underset{\sim}{\boldsymbol{\sigma}} : \underset{\sim}{\boldsymbol{P}}^\alpha = \underset{\sim}{\boldsymbol{\sigma}}^s : \underset{\sim}{\boldsymbol{P}}^{\alpha s} + \underset{\sim}{\boldsymbol{\sigma}}^a : \underset{\sim}{\boldsymbol{P}}^{\alpha a} = \tau^\alpha_{sym} - \chi^\alpha, \tag{20}$$

where $\underset{\sim}{\boldsymbol{P}}^{\alpha}=\underline{\boldsymbol{l}}^{\alpha}\otimes\underline{\boldsymbol{n}}^{\alpha}$ is the orientation tensor. The first term in the generalised resolved shear stress is the classical resolved shear stress τ^{α}_{sym}. The second term is a back stress, x^{α}, which is related to the divergence of the couple stress tensor. Recalling Eq. (11):

$$x^{\alpha}=-\frac{1}{2}(\mathrm{div}\,\underset{\sim}{\boldsymbol{m}})\cdot(\underline{\boldsymbol{l}}^{\alpha}\times\underline{\boldsymbol{n}}^{\alpha}). \tag{21}$$

The slip system is activated when the resolved shear stress reaches the threshold, τ_c, so that the yield criterion reads

$$|\tau^{\alpha}|=|\tau^{\alpha}_{sym}-x^{\alpha}|\le\tau_c. \tag{22}$$

It has been shown in Forest (2008) that this back stress component leads to linear kinematic hardening in single slip under simple shear.

2.2. Application to a two-phase periodic microstructure under simple shear

We consider a two-phase periodic microstructure under simple shear as studied in Forest and Sedláček (2003) and Forest (2008). This microstructure, described in Fig. 2, is composed of a hard purely elastic phase (h) and a soft elasto-plastic single crystal phase (s). One single slip system is considered in the soft phase (s), with slip direction normal to the interface plane (h)/(s). This periodic unit cell is subjected to a mean simple glide $\overline{\gamma}$ in the crystal slip direction of the phase (s). We look for a displacement and micro-rotation fields of the form

$$u_1=\overline{\gamma}x_2,\quad u_2(x_1)=u(x_1),\quad u_3=0, \tag{23}$$

$$\phi_1=\phi_2=0,\quad \phi_3=\phi(x_1). \tag{24}$$

Consequently, the Cosserat deformation and curvature tensors become

$$\underset{\sim}{\boldsymbol{e}}=\begin{bmatrix}0 & \overline{\gamma}+\phi(x_1) & 0\\ u_{,1}-\phi(x_1) & 0 & 0\\ 0 & 0 & 0\end{bmatrix},\quad \underset{\sim}{\boldsymbol{\kappa}}=\begin{bmatrix}0 & 0 & 0\\ 0 & 0 & 0\\ \phi_{,1} & 0 & 0\end{bmatrix} \tag{25}$$

The solution for $\underline{\boldsymbol{\phi}}$ in the elastic phase (h) can be found in Forest and Sedláček (2003). The micro-rotation exhibits a hyperbolic profile, given by

$$\phi^{(h+)}=a^h\cosh\left(\omega^h\left(x_1-\frac{s+h}{2}\right)\right)+d^h\quad\text{for } s/2<x<(s+h)/2, \tag{26}$$

$$\phi^{(h-)}=a^h\cosh\left(\omega^h\left(x_1+\frac{s+h}{2}\right)\right)+d^h\quad\text{for } -(s+h)/2<x<-s/2, \tag{27}$$

with

$$\omega^{h2}=\frac{2\mu^h\mu^h_c}{\beta^h(\mu^h+\mu^h_c)}, \tag{28}$$

and with a^h and d^h being two integration constants. The following relations are obtained for the deformation tensor:

$$e^{(h+)}_{21}=-\frac{\mu^h-\mu^h_c}{\mu^h+\mu^h_c}\phi^{h+}+\overline{\gamma}+d^h\frac{2\mu^h}{\mu^h+\mu^h_c}, \tag{29}$$

$$e^{(h-)}_{21}=-\frac{\mu^h-\mu^h_c}{\mu^h+\mu^h_c}\phi^{h-}+\overline{\gamma}+d^h\frac{2\mu^h}{\mu^h+\mu^h_c}. \tag{30}$$

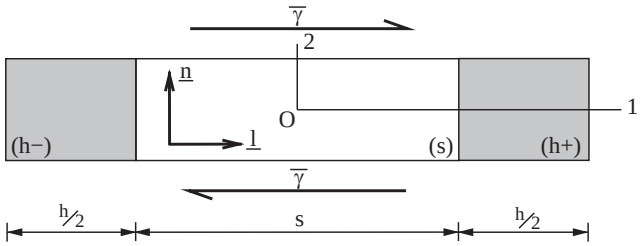

Fig. 2. Single slip in a two-phase periodic microstructure under simple shear: the grey phase (h) displays a purely linear elastic behaviour whereas the inelastic deformation of the white elasto-plastic phase (s) is controlled by a single slip system ($\underline{\boldsymbol{n}},\underline{\boldsymbol{l}}$).

In the plastic phase, the solution is derived here for the yield criterion (22). We compute successively,

$$\underset{\sim}{\boldsymbol{e}}^p = \gamma \underline{\boldsymbol{l}} \otimes \underline{\boldsymbol{n}} = \begin{bmatrix} 0 & \gamma & 0 \\ 0 & 0 & 0 \\ 0 & 0 & 0 \end{bmatrix}, \quad \underset{\sim}{\boldsymbol{e}}^e = \begin{bmatrix} 0 & e^e_{12} & 0 \\ e^e_{21} & 0 & 0 \\ 0 & 0 & 0 \end{bmatrix}, \tag{31}$$

which results into two non-zero components for the stress tensor,

$$\sigma_{12} = \mu^s(e^e_{12}+e^e_{21}) + \mu^s_c(e^e_{12}-e^e_{21}), \tag{32}$$

$$\sigma_{21} = \mu^s(e^e_{12}+e^e_{21}) + \mu^s_c(e^e_{21}-e^e_{12}), \tag{33}$$

and one non-zero component for the couple-stress tensor,

$$m_{31} = 2\beta^s \kappa_{31}. \tag{34}$$

The balance equations yield

$$\sigma_{21,1} = 0, \tag{35}$$

$$m_{31,1} - (\sigma_{12}-\sigma_{21}) = 0. \tag{36}$$

The resolved shear stress is given by

$$\tau = \underset{\sim}{\boldsymbol{\sigma}} : \underset{\sim}{\boldsymbol{P}} = \sigma_{12}. \tag{37}$$

Combining Eqs. (35)–(37) and the yield condition (22), we obtain the following equation for the micro-rotation axial vector in the (s) phase

$$\phi^s_{,111} = 0. \tag{38}$$

The integration of Eq. (38) leads to a parabolic profile for ϕ^s

$$\phi^s = a^s x_1^2 + d^s, \tag{39}$$

where a^s and d^s are two integration constants.

The determination of the four integration constants, a^s, d^s, a^h, d^h, is done after taking interface and periodicity boundary conditions into account:

- Continuity of ϕ at $x_1 = s/2$:

$$a^s \frac{s^2}{4} + d^s = a^h \cosh\left(\omega^h \frac{h}{2}\right) + d^h. \tag{40}$$

- Continuity of m_{31} at $x_1 = s/2$:

$$\beta^s a^s s = -\beta^h a^h \omega^h \sinh\left(\omega^h \frac{h}{2}\right). \tag{41}$$

- Continuity of σ_{21} at $x_1 = s/2$ in the phase (s),

$$\sigma_{21} = m_{31,1} + \sigma_{12}, \tag{42}$$

which implies that

$$\sigma_{21} = 4\beta^s a^s + \tau_c. \tag{43}$$

In the phase (h), one finds that

$$\sigma_{21} = \mu^h(\overline{\gamma}+\phi+e_{21}) + \mu^h_c(\overline{\gamma}+\phi-e_{21}) = 2\mu^h(\overline{\gamma}+d^h). \tag{44}$$

Combining the two previous equations, we obtain

$$4\beta^s a^s + \tau_c = 2\mu^h(\overline{\gamma}+d^h). \tag{45}$$

- Periodicity of u_2. We use the property $\langle e_{21} \rangle = \langle u_{,1} - \phi \rangle = -\langle \phi \rangle$.

In the phase (h), one finds

$$e_{21} = \frac{2\mu^h_c}{\mu^h+\mu^h_c} a^h \cosh\left(\omega^h\left(x_1 - \frac{s+h}{2}\right)\right) + \overline{\gamma} + 2d^h, \tag{46}$$

and in the phase (s):

$$e_{21} = e^e_{21} = \frac{\tau_c}{2\mu} + \frac{\beta^s a^s(\mu^s+\mu^s_c)}{\mu^s \mu^s_c}, \tag{47}$$

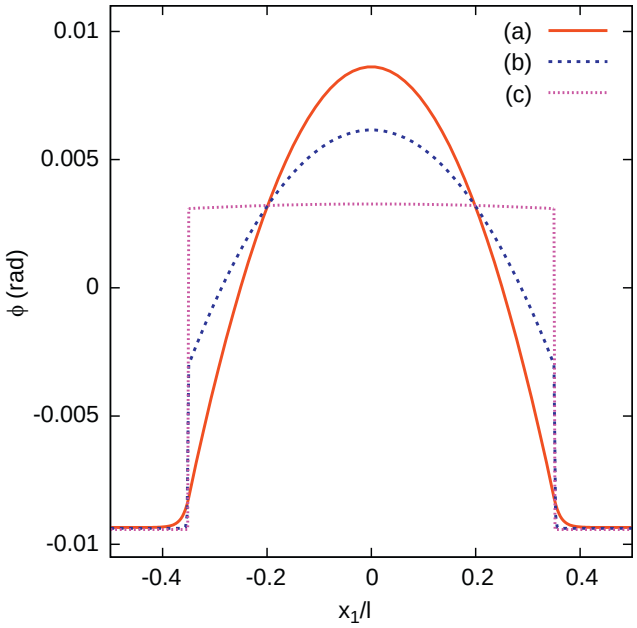

Fig. 3. Profiles of the lattice rotation angle ϕ (rad) in the two-phase microstructure predicted by the Cosserat model: (a) with a set of material parameters giving clearly visible parabolic and hyperbolic profiles ($\mu = 35\,000$ MPa, $\mu_c^h = \mu_c^s = 10^6$ MPa, $\beta^h = \beta^s = 10^{-5}$ MPa mm^2 and $\tau_c = 40$ MPa), (b) with a stronger mismatch between the moduli of the two phases $\beta^h = 10^{-7}$ MPa mm^2 and $\beta^s = 10^{-5}$ MPa mm^2 and (c) $\beta^h = 10^{-11}$ MPa mm^2 and $\beta^s = 10^{-5}$ MPa mm^2, which leads to sharper interface profiles. In all three cases, f_s=0.7 and the $\beta^{h,s}$ values are chosen for $l = 1$ μm.

which gives the following relationships between the integration constants:

$$s\left(\frac{\tau_c}{2\mu} - \frac{\beta^s a^s(\mu^s+\mu_c^s)}{\mu^s\mu_c^s} + d^s\right) + a^s\frac{s^3}{12} + \frac{4\mu_c^h a^h}{\mu^h+\mu_c^h}\sinh\left(\omega^h\frac{h}{2}\right) + h(2d^h+\overline{\gamma}) = 0. \tag{48}$$

By solving Eqs. (40)–(48) analytically, the following expression for the constant a^s is obtained:

$$a^s = \frac{\overline{\gamma} - \frac{\tau_c}{2\mu^h}\left(f_s + 2(1-f_s) + f_s\frac{\mu^h}{\mu^s}\right)}{-\frac{f_s^3}{6}l^2 - \beta^s\frac{f_s^2}{\beta^h\omega^h}l\coth\left(\omega^h\frac{l(1-f_s)}{2}\right) - \beta^s\left(f_s\frac{\mu^s+\mu_c^s}{\mu^s\mu_c^s} + \frac{4}{\mu^h}\right)}. \tag{49}$$

In Eq. (49), f_s represents the fraction of phase (s), f_s=s/l. The remaining constants can be determined in terms of a^s:

$$a^h = \frac{-s\beta^s a^s}{\beta^h\omega^h\sinh(\omega^h\frac{h}{2})}, \tag{50}$$

$$d^h = -\frac{4\beta^s a^s - \tau_c}{2\mu^h} - \overline{\gamma}, \tag{51}$$

$$d^s = -\frac{4\beta^s a^s - \tau_c}{2\mu^h} - \overline{\gamma} - \frac{s\beta^s a^s}{\beta^h\omega^h}\coth\left(\omega^h\frac{h}{2}\right) - a^s\frac{s^2}{4}. \tag{52}$$

Fig. 3 illustrates the micro-rotation profile in the two-phase laminate for a fraction of phase (s) equal to 0.7, and for three different sets of material parameters. The first one clearly shows the continuity of the micro-rotation at the interface while the two others, introducing a stronger mismatch between the two phases, show sharper profiles at the interfaces. The set of material parameters (a) has been chosen in order to clearly show the parabolic profile in the soft phase and the hyperbolic one in the hard phase. Note that if l is changed into $l/10$, values of $\beta^{h,s}/100$ will provide the same curves.

3. Strain gradient plasticity: the "*curl* H^p" model

We consider now a strain gradient plasticity theory which includes the full curl of the plastic deformation tensor, $\underset{\sim}{\boldsymbol{H}}^p$. This approach, herefrom to be referred to as the "*curl* H^p" model, was proposed by Gurtin (2002) and applied to a constrained layer and a composite problem in Bittencourt et al. (2003). The balance and constitutive equations are first recalled and recast into the notations used throughout this work. Then the model is applied to a crystal undergoing single slip. It will be shown that a specific form of the back stress arises from this application. As it was done with the Cosserat model, the "*curl* H^p" model is finally applied to the two-phase microstructure illustrated in Fig. 2.

3.1. Balance equations

Following Gurtin (2002), we consider a continuum whose power density of internal forces takes the form

$$p^{(i)} = \underset{\sim}{\boldsymbol{\sigma}} : \dot{\underset{\sim}{\boldsymbol{H}}} + \underset{\sim}{\boldsymbol{s}} : \dot{\underset{\sim}{\boldsymbol{H}}}^{p} + \underset{\sim}{\boldsymbol{M}} : \operatorname{curl} \dot{\underset{\sim}{\boldsymbol{H}}}^{p}. \tag{53}$$

For objectivity reasons, the stress tensor $\underset{\sim}{\boldsymbol{\sigma}}$ is symmetric whereas the micro-stress tensor $\underset{\sim}{\boldsymbol{s}}$ and the double-stress tensor $\underset{\sim}{\boldsymbol{M}}$ are generally asymmetric. The total power of internal forces in a domain V, with boundary ∂V, is

$$\begin{aligned}\mathcal{P}^{(i)} &= \int_V (\underset{\sim}{\boldsymbol{\sigma}} : \dot{\underset{\sim}{\boldsymbol{H}}} + \underset{\sim}{\boldsymbol{s}} : \dot{\underset{\sim}{\boldsymbol{H}}}^{p} + \underset{\sim}{\boldsymbol{M}} : \operatorname{curl} \dot{\underset{\sim}{\boldsymbol{H}}}^{p})\, dV = \int_V ((\sigma_{ij}\dot{u}_i)_{,j} + (M_{ij}\epsilon_{jkl}\dot{H}^p_{ik})_{,l})\, dV + \int_V (-\sigma_{ij,j}\dot{u}_i + s_{ij}\dot{H}^p_{ij} - \epsilon_{jkl}M_{ij,l}\dot{H}^p_{ik})\, dV \\ &= -\int_V (\sigma_{ij,j}\dot{u}_i - (\epsilon_{kjl}M_{ik,l} - s_{ij})\dot{H}^p_{ij})\, dV + \int_{\partial V} \left(\sigma_{ij} n_j \dot{u}_i + \int_{\partial V} \epsilon_{jkl} M_{ij} n_l \dot{H}^p_{ik} \right) dS.\end{aligned}$$

The power density of contact forces is taken as

$$p^{(c)} = \underline{\boldsymbol{t}} \cdot \dot{\underline{\boldsymbol{u}}} + \underset{\sim}{\boldsymbol{m}} : \dot{\underset{\sim}{\boldsymbol{H}}}^{p}, \tag{54}$$

where $\underline{\boldsymbol{t}}$, $\underset{\sim}{\boldsymbol{m}}$ are, respectively, the surface simple and double tractions. Volume forces are not written for simplicity. The method of virtual power can be used to derive the field equations governing the continuum, based on the virtual motions $\dot{\underline{\boldsymbol{u}}}$ and $\dot{\underset{\sim}{\boldsymbol{H}}}^{p}$:

$$\operatorname{div} \underset{\sim}{\boldsymbol{\sigma}} = 0, \quad \sigma_{ij,j} = 0, \tag{55}$$

$$\operatorname{curl} \underset{\sim}{\boldsymbol{M}} + \underset{\sim}{\boldsymbol{s}} = 0, \quad \epsilon_{jkl} M_{ik,l} + s_{ij} = 0, \tag{56}$$

for all regular points of the domain V. Furthermore, the following boundary conditions on ∂V can be derived:

$$\underline{\boldsymbol{t}} = \underset{\sim}{\boldsymbol{\sigma}} \cdot \underline{\boldsymbol{n}}, \quad t_i = \sigma_{ij} n_j, \tag{57}$$

$$\underset{\sim}{\boldsymbol{m}} = \underset{\sim}{\boldsymbol{M}} \cdot \underset{\sim}{\boldsymbol{\varepsilon}} \cdot \underline{\boldsymbol{n}}, \quad m_{ij} = M_{ik}\epsilon_{kjl} n_l. \tag{58}$$

3.2. Energy and entropy principles: constitutive equations

Under isothermal conditions, the energy balance in its local form states that

$$\rho \dot{e} = p^{(i)}, \tag{59}$$

where e is the internal energy density function and ρ the mass density. The entropy principle is formulated as

$$\rho(\dot{e} - \dot{\psi}) \geq 0 \tag{60}$$

where ψ is the Helmholtz free energy function. The free energy is taken as a function of the elastic strain, $\underset{\sim}{\boldsymbol{\varepsilon}}^e$, the dislocation density tensor, or $\operatorname{curl} \underset{\sim}{\boldsymbol{H}}^p$, and a generic internal hardening variable, q, viz. $\psi(\underset{\sim}{\boldsymbol{\varepsilon}}^e, \operatorname{curl} \underset{\sim}{\boldsymbol{H}}^p, q)$. As a result, the Clausius–Duhem inequality becomes

$$\left(\underset{\sim}{\boldsymbol{\sigma}} - \rho \frac{\partial \psi}{\partial \underset{\sim}{\boldsymbol{\varepsilon}}^e} \right) : \dot{\underset{\sim}{\boldsymbol{\varepsilon}}}^e + \left(\underset{\sim}{\boldsymbol{M}} - \rho \frac{\partial \psi}{\partial \operatorname{curl} \underset{\sim}{\boldsymbol{H}}^p} \right) : \operatorname{curl} \dot{\underset{\sim}{\boldsymbol{H}}}^p + (\underset{\sim}{\boldsymbol{\sigma}} + \underset{\sim}{\boldsymbol{s}}) : \dot{\underset{\sim}{\boldsymbol{H}}}^p - \rho \frac{\partial \psi}{\partial q} \dot{q} \geq 0. \tag{61}$$

Here, the constitutive assumption is made that the two first terms in the previous inequality are non-dissipative and therefore should vanish. Then,

$$\underset{\sim}{\boldsymbol{\sigma}} = \rho \frac{\partial \psi}{\partial \underset{\sim}{\boldsymbol{\varepsilon}}^e}, \quad \underset{\sim}{\boldsymbol{M}} = \rho \frac{\partial \psi}{\partial \operatorname{curl} \underset{\sim}{\boldsymbol{H}}^p}. \tag{62}$$

It follows that the residual dissipation rate is

$$D = (\underset{\sim}{\boldsymbol{\sigma}} + \underset{\sim}{\boldsymbol{s}}) : \dot{\underset{\sim}{\boldsymbol{H}}}^p - R\dot{q} \geq 0, \tag{63}$$

where $R = \rho \partial \psi / \partial q$ is the thermodynamic force associated with the internal variable, q. The existence of a dissipation potential, namely $\Omega(\underset{\sim}{\boldsymbol{\sigma}} + \underset{\sim}{\boldsymbol{s}}, R)$, is postulated so that

$$\dot{\underset{\sim}{\boldsymbol{H}}}^p = \frac{\partial \Omega}{\partial (\underset{\sim}{\boldsymbol{\sigma}} + \underset{\sim}{\boldsymbol{s}})}, \quad \dot{q} = -\frac{\partial \Omega}{\partial R}. \tag{64}$$

3.3. Application of the "curlH^p" model to a single slip problem

For a crystal deforming under single slip conditions, the plastic deformation rate is given by

$$\dot{\underset{\sim}{\boldsymbol{H}}}^p = \dot{\gamma}\underset{\sim}{\boldsymbol{P}} = \dot{\gamma}\,\underline{\boldsymbol{l}} \otimes \underline{\boldsymbol{n}}, \tag{65}$$

where $\underset{\sim}{\boldsymbol{P}} = \underline{\boldsymbol{l}} \otimes \underline{\boldsymbol{n}}$ is the orientation tensor, $\underline{\boldsymbol{l}}$ is the slip direction and $\underline{\boldsymbol{n}}$ the normal to the slip plane. The dissipation rate can then be expressed as

$$(\tau + \underline{\boldsymbol{l}} \cdot \underset{\sim}{\boldsymbol{s}} \cdot \underline{\boldsymbol{n}})\dot{\gamma} - R\dot{q} \geq 0, \tag{66}$$

where $\tau = \underline{\boldsymbol{l}} \cdot \underset{\sim}{\boldsymbol{\sigma}} \cdot \underline{\boldsymbol{n}}$ is the resolved shear stress. In the absence of a hardening variable, q, for simplicity, the following generalised Schmid law can be defined (for positive $\dot{\gamma}$):

$$|\tau - x| = \tau_c \quad \text{with } x = -\underline{\boldsymbol{l}} \cdot \underset{\sim}{\boldsymbol{s}} \cdot \underline{\boldsymbol{n}}, \tag{67}$$

meaning that plastic flow occurs when the effective resolved shear stress $|\tau - x|$ reaches the critical resolved shear stress τ_c. A kinematic hardening component, x, naturally arises in the formulation for which a more specific form is given next. The curl of the plastic deformation is then given by

$$\operatorname{curl} \underset{\sim}{\boldsymbol{H}}^p = \underline{\boldsymbol{l}} \otimes (\underline{\boldsymbol{n}} \times \boldsymbol{\nabla}\gamma). \tag{68}$$

For a two-dimensional case, one finds

$$[\operatorname{curl} \underset{\sim}{\boldsymbol{H}}^p] = \begin{bmatrix} 0 & 0 & \gamma_{,2} n_1 n_2 - \gamma_{,1} n_2^2 \\ 0 & 0 & -\gamma_{,2} n_1^2 + \gamma_{,1} n_1 n_2 \\ 0 & 0 & 0 \end{bmatrix}. \tag{69}$$

In the particular case when $\underline{\boldsymbol{l}} = \underline{\boldsymbol{e}}_1, \underline{\boldsymbol{n}} = \underline{\boldsymbol{e}}_2$, the only non-vanishing component of the dislocation density tensor is

$$(\operatorname{curl} \underset{\sim}{\boldsymbol{H}}^p)_{13} = -\gamma_{,1}. \tag{70}$$

Let us consider at this stage the simple quadratic potential:

$$\rho\psi(\underset{\sim}{\boldsymbol{\varepsilon}}^e, \operatorname{curl} \underset{\sim}{\boldsymbol{H}}^p) = \frac{1}{2}\,\underset{\sim}{\boldsymbol{\varepsilon}}^e : \underset{\approx}{\boldsymbol{\Lambda}} : \underset{\sim}{\boldsymbol{\varepsilon}}^e + \frac{1}{2} A (\operatorname{curl} \underset{\sim}{\boldsymbol{H}}^p) : (\operatorname{curl} \underset{\sim}{\boldsymbol{H}}^p), \tag{71}$$

so that

$$\underset{\sim}{\boldsymbol{\sigma}} = \underset{\approx}{\boldsymbol{\Lambda}} : \underset{\sim}{\boldsymbol{\varepsilon}}^e, \quad \underset{\sim}{\boldsymbol{M}} = A \operatorname{curl} \underset{\sim}{\boldsymbol{H}}^p, \tag{72}$$

where $\underset{\approx}{\boldsymbol{\Lambda}}$ is the four-rank tensor of the elastic moduli, assumed isotropic hereafter, and A is a higher order modulus. According to the balance equation (56), it follows that

$$\underset{\sim}{\boldsymbol{s}} = -\operatorname{curl} \underset{\sim}{\boldsymbol{M}} = -\operatorname{curl} \operatorname{curl} \underset{\sim}{\boldsymbol{H}}^p. \tag{73}$$

For single slip, the double curl of plastic deformation is defined as

$$\operatorname{curl} \operatorname{curl} \underset{\sim}{\boldsymbol{H}}^p = \underline{\boldsymbol{l}} \otimes ((\underline{\boldsymbol{n}} \times \gamma_{,ij} \underline{\boldsymbol{e}}_i) \times \underline{\boldsymbol{e}}_j). \tag{74}$$

In the particular case of $\underline{\boldsymbol{l}} = \underline{\boldsymbol{e}}_1, \underline{\boldsymbol{n}} = \underline{\boldsymbol{e}}_2$, we obtain

$$\operatorname{curl} \operatorname{curl} \underset{\sim}{\boldsymbol{H}}^p = \gamma_{,12} \underline{\boldsymbol{e}}_1 \otimes \underline{\boldsymbol{e}}_1 - \gamma_{,11} \underline{\boldsymbol{e}}_1 \otimes \underline{\boldsymbol{e}}_2, \tag{75}$$

so that the back stress takes the form

$$x = A(\operatorname{curl} \operatorname{curl} \underset{\sim}{\boldsymbol{H}}^p) : (\underline{\boldsymbol{l}} \otimes \underline{\boldsymbol{n}}) = -A\gamma_{,11}. \tag{76}$$

3.4. Application to a two-phase periodic microstructure under simple shear

We consider the same two-phase periodic microstructure under simple shear illustrated in Fig. 2. When the previously described "*curl* H^p" continuum plasticity theory is applied to the laminate problem shown in Section 2.2, the main unknowns are the component of displacement, u_2, and the H^p_{12} component of plastic deformation:

$$u_1 = \overline{\gamma} x_2, \quad u_2(x_1) = u(x_1), \quad u_3 = 0, \quad H^p_{12}(x_1). \tag{77}$$

Recalling,

$$\underset{\sim}{\boldsymbol{H}}^p = \gamma \underline{\boldsymbol{l}} \otimes \underline{\boldsymbol{n}} = \gamma \underline{\boldsymbol{e}}_1 \otimes \underline{\boldsymbol{e}}_2, \tag{78}$$

we obtain

$$[\underset{\sim}{\boldsymbol{H}}]=\begin{bmatrix}0 & \overline{\gamma} & 0\\ u_{,1} & 0 & 0\\ 0 & 0 & 0\end{bmatrix},\quad [\underset{\sim}{\boldsymbol{H}}^p]=\begin{bmatrix}0 & \gamma & 0\\ 0 & 0 & 0\\ 0 & 0 & 0\end{bmatrix},\quad [\underset{\sim}{\boldsymbol{H}}^e]=\begin{bmatrix}0 & \overline{\gamma}-\gamma & 0\\ u_{,1} & 0 & 0\\ 0 & 0 & 0\end{bmatrix} \tag{79}$$

$$[\operatorname{curl}\underset{\sim}{\boldsymbol{H}}^p]=\begin{bmatrix}0 & 0 & -\gamma_{,1}\\ 0 & 0 & 0\\ 0 & 0 & 0\end{bmatrix}. \tag{80}$$

The resulting stress tensors are

$$[\underset{\sim}{\boldsymbol{\sigma}}]=\mu\begin{bmatrix}0 & \overline{\gamma}-\gamma+u_{,1} & 0\\ \overline{\gamma}-\gamma+u_{,1} & 0 & 0\\ 0 & 0 & 0\end{bmatrix},\quad [\underset{\sim}{\boldsymbol{M}}]=A\begin{bmatrix}0 & 0 & -\gamma_{,1}\\ 0 & 0 & 0\\ 0 & 0 & 0\end{bmatrix}, \tag{81}$$

$$[\operatorname{curl}\underset{\sim}{\boldsymbol{M}}]=A\begin{bmatrix}0 & -\gamma_{,11} & 0\\ 0 & 0 & 0\\ 0 & 0 & 0\end{bmatrix}. \tag{82}$$

The balance equations (55) and (56) imply that

$$\sigma_{12,1}=0 \implies -\gamma_{,1}+u_{,11}=0, \tag{83}$$

and

$$s_{12}=-(\operatorname{curl}\underset{\sim}{\boldsymbol{M}})_{12} \implies s_{12}=A\gamma_{,11}. \tag{84}$$

Thus, the shear stress component, σ_{12}, is constant. For this particular case, Schmid law is written as

$$\tau-x=\sigma_{12}-x=\tau_c, \tag{85}$$

with

$$x=A(\operatorname{curl}\operatorname{curl}\underset{\sim}{\boldsymbol{H}}^p)_{12}=-A\gamma_{,11}. \tag{86}$$

As the shear stress σ_{12} is constant, so is the corresponding back stress,

$$x_{,1}=\gamma_{,111}=0. \tag{87}$$

The slip profile is therefore parabolic in the plastic phase. In the elastic zone, all the variables, H^p_{12},M_{13},γ,x, vanish.

We now enforce continuity requirements at the interface between both phases for the plastic slip, in addition to the continuity of displacement and simple traction vector. The continuity condition of plastic slip at $x_1 = \pm s/2$ is

$$H^p_{12}=\gamma=0. \tag{88}$$

The condition of continuity of the double traction tensor, (58), at the interface needs to be considered next. Here,

$$m_{12}=M_{13}\varepsilon_{321}n_1=-M_{13}=A\gamma_{,1}, \tag{89}$$

which implies the continuity of the double stress component, M_{13}. In the elastic phase, the couple stress component M_{13} is not defined since no plastic deformation takes place. If we impose the condition that $M_{13} = m_{12} = 0$ at the interface, it will imply that the first derivative, $\gamma_{,1}$, also vanishes. This latter condition requires that the full parabolic function γ should also vanish, so that no plastic strain could develop in the plastic zone. In fact, according to such a plastic strain gradient model, higher order stresses exhibit a jump at the interface between an elastic and a plastic phase. This discontinuity of the generalized traction prompts us to introduce, in the next section, a regularised model which is closely related to the "*curl* H^p" model but which offers a complete solution to the elastic/plastic laminate boundary value problem. On the other hand, it must be noted that a complete solution can be worked out with the "*curl* H^p" model when both phases are elasto-plastic (see Appendix B). The regularised model presented next will give us a way to find a valid interface condition and to derive the jump condition for generalized tractions (see Appendix C).

4. Formulation of the *microcurl* model

An alternative model will now be proposed in order to circumvent the discontinuity of the generalized traction observed in the boundary value problem of interest, thus representing a regularisation of the "*curl* H^p" model. This model, called here *microcurl*, is based on a micromorphic approach that falls in the class of generalised continuum models presented in Forest (2009). The theory is first described in terms of the balance and constitutive equations. An internal constraint controlling the plastic micro-deformation is then introduced. Finally an application of the model to the two-phase laminate problem of Fig. 2 is

presented. Finally, it will be shown that the "*curl* H^p" model can be obtained as a special limiting case of the *microcurl* formulation proposed here.

4.1. Balance equations

We introduce a plastic micro-deformation variable, $\underset{\sim}{\boldsymbol{\chi}}^p$, as a second-rank generally non-symmetric tensor. It is distinct from the plastic deformation $\underset{\sim}{\boldsymbol{H}}^p$ which is still treated as an internal variable. Then the degrees of freedom of the theory are

$$DOF = \{\underline{\boldsymbol{u}}, \underset{\sim}{\boldsymbol{\chi}}^p\} \tag{90}$$

The components of $\underset{\sim}{\boldsymbol{\chi}}^p$ are introduced as independent degrees of freedom. In the three-dimensional case, there are nine such components and the micro-deformation field is generally incompatible. We assume that only the curl part of the gradient of plastic micro-deformation plays a role in the power of internal forces. Then, in the same way as in Eq. (53), we assume that

$$p^{(i)} = \underset{\sim}{\boldsymbol{\sigma}} : \dot{\underset{\sim}{\boldsymbol{H}}} + \underset{\sim}{\boldsymbol{s}} : \dot{\underset{\sim}{\boldsymbol{\chi}}}^p + \underset{\sim}{\boldsymbol{M}} : \operatorname{curl} \dot{\underset{\sim}{\boldsymbol{\chi}}}^p. \tag{91}$$

The total power of internal forces over the domain V is then given by

$$\begin{aligned} -\mathcal{P}^{(i)} &= \int_V p^{(i)}\, dV = \int_V (\underset{\sim}{\boldsymbol{\sigma}} : \dot{\underset{\sim}{\boldsymbol{H}}} + \underset{\sim}{\boldsymbol{s}} : \dot{\underset{\sim}{\boldsymbol{\chi}}}^p + \underset{\sim}{\boldsymbol{M}} : \operatorname{curl} \dot{\underset{\sim}{\boldsymbol{\chi}}}^p)\, dV, \\ &= \int_V ((\sigma_{ij}\dot{u}_i)_{,j} + (M_{ij}\epsilon_{jkl}\dot{\chi}^p_{ik})_{,l})\, dV + \int_V (-\sigma_{ij,j}\dot{u}_i + s_{ij}\dot{\chi}^p_{ij} - \epsilon_{jkl}M_{ij,l}\dot{\chi}^p_{ik})\, dV, \\ &= -\int_V \sigma_{ij,j}\dot{u}_i\, dV - \int_V (\epsilon_{kjl}M_{ik,l} - s_{ij})\dot{\chi}^p_{ij}\, dV + \int_{\partial V} \sigma_{ij} n_j \dot{u}_i\, dS + \int_{\partial V} \epsilon_{jkl} M_{ij} n_l \dot{\chi}^p_{ik}\, dS. \end{aligned}$$

The method of virtual power is used to derive the generalised balance of momentum equations. Assuming no volume forces for simplicity, one finds

$$\operatorname{div} \underset{\sim}{\boldsymbol{\sigma}} = 0, \quad \operatorname{curl} \underset{\sim}{\boldsymbol{M}} + \underset{\sim}{\boldsymbol{s}} = 0. \tag{92}$$

The corresponding boundary conditions are

$$\underline{\boldsymbol{t}} = \underset{\sim}{\boldsymbol{\sigma}} \cdot \underline{\boldsymbol{n}}, \quad \underline{\boldsymbol{m}} = \underset{\sim}{\boldsymbol{M}} \cdot \underset{\sim}{\boldsymbol{\epsilon}} \cdot \underline{\boldsymbol{n}}, \tag{93}$$

where $\underline{\boldsymbol{t}}$ and $\underline{\boldsymbol{m}}$ are the simple and double tractions at the boundary.

4.2. Constitutive equations

The free energy function is assumed to have the following arguments:

$$\psi(\underset{\sim}{\boldsymbol{\varepsilon}}^e, \underset{\sim}{\boldsymbol{e}}^p \coloneqq \underset{\sim}{\boldsymbol{H}}^p - \underset{\sim}{\boldsymbol{\chi}}^p, \underset{\sim}{\boldsymbol{\Gamma}}_{\chi} \coloneqq \operatorname{curl} \underset{\sim}{\boldsymbol{\chi}}^p) \tag{94}$$

where $\underset{\sim}{\boldsymbol{e}}^p$ is the relative plastic strain measuring the difference between plastic deformation and the plastic microvariable.

The reduced entropy inequality reads

$$\left(\underset{\sim}{\boldsymbol{\sigma}} - \rho \frac{\partial \psi}{\partial \underset{\sim}{\boldsymbol{\varepsilon}}^e}\right) : \dot{\underset{\sim}{\boldsymbol{\varepsilon}}}^e - \left(\underset{\sim}{\boldsymbol{s}} + \rho \frac{\partial \psi}{\partial \underset{\sim}{\boldsymbol{e}}^p}\right) : \dot{\underset{\sim}{\boldsymbol{e}}}^p + \left(\underset{\sim}{\boldsymbol{M}} - \rho \frac{\partial \psi}{\partial \underset{\sim}{\boldsymbol{\Gamma}}_{\chi}}\right) : \dot{\underset{\sim}{\boldsymbol{\Gamma}}}_{\chi} + (\underset{\sim}{\boldsymbol{\sigma}} + \underset{\sim}{\boldsymbol{s}}) : \dot{\underset{\sim}{\boldsymbol{H}}}^p \geq 0. \tag{95}$$

Furthermore, the following state laws are adopted:

$$\underset{\sim}{\boldsymbol{\sigma}} = \rho \frac{\partial \psi}{\partial \underset{\sim}{\boldsymbol{\varepsilon}}^e}, \quad \underset{\sim}{\boldsymbol{s}} = -\rho \frac{\partial \psi}{\partial \underset{\sim}{\boldsymbol{e}}^p}, \quad \underset{\sim}{\boldsymbol{M}} = \rho \frac{\partial \psi}{\partial \underset{\sim}{\boldsymbol{\Gamma}}_{\chi}}, \tag{96}$$

so that the residual intrinsic dissipation rate is defined as

$$D = (\underset{\sim}{\boldsymbol{\sigma}} + \underset{\sim}{\boldsymbol{s}}) : \dot{\underset{\sim}{\boldsymbol{H}}}^p \geq 0. \tag{97}$$

Assuming a quadratic potential in Eq. (96), the following linear relationships are obtained:

$$\underset{\sim}{\boldsymbol{\sigma}} = \underset{\approx}{\boldsymbol{\Lambda}} : \underset{\sim}{\boldsymbol{\varepsilon}}^e, \quad \underset{\sim}{\boldsymbol{s}} = -H_\chi \underset{\sim}{\boldsymbol{e}}^p, \quad \underset{\sim}{\boldsymbol{M}} = A \underset{\sim}{\boldsymbol{\Gamma}}_{\chi}, \tag{98}$$

where H_χ and A are the generalised moduli. The size effects exhibited by the solutions of boundary value problems involving such a model are related to an intrinsic length scale, typically defined as

$$l_\omega = \sqrt{\frac{A}{H_\chi}}. \tag{99}$$

The flow rule can be derived from a viscoplastic potential, $\Omega(\underset{\sim}{\boldsymbol{\sigma}}+\underset{\sim}{\boldsymbol{s}})$, expressed in terms of the effective stress, $(\underset{\sim}{\boldsymbol{\sigma}}+\underset{\sim}{\boldsymbol{s}})$, that intervenes in the dissipation rate, see Eq. (97). Then,

$$\dot{\underset{\sim}{\boldsymbol{H}}}^p = \frac{\partial \Omega}{\partial(\underset{\sim}{\boldsymbol{\sigma}}+\underset{\sim}{\boldsymbol{s}})} \tag{100}$$

For a crystal undergoing single slip, Eq. (65) is still valid. The dissipation takes the form

$$D = (\tau + \underset{\sim}{\boldsymbol{s}} : (\underline{\boldsymbol{l}} \otimes \underline{\boldsymbol{n}}))\dot{\gamma} \geq 0 \tag{101}$$

The generalised Schmid criterion then becomes

$$|\tau + \underset{\sim}{\boldsymbol{s}} : (\underline{\boldsymbol{l}} \otimes \underline{\boldsymbol{n}})| = \tau_c, \tag{102}$$

where τ_c is the critical resolved shear stress. Accordingly, a back stress component naturally arises in the yield function $f(\tau, \underset{\sim}{\boldsymbol{s}}) = |\tau + \underset{\sim}{\boldsymbol{s}} : (\underline{\boldsymbol{l}} \otimes \underline{\boldsymbol{n}})| - \tau_c$, in the same way as in the Cosserat and "*curl* H^p" models.

4.3. Internal constraint

The modulus H_χ in Eq. (98) introduces a coupling between the macro and micro-variables. It could also be interpreted as a penalty factor that constrains the relative plastic deformation $\underset{\sim}{\boldsymbol{e}}^p$ to remain sufficiently small. Equivalently, a high value of the coupling modulus, H_χ, forces the plastic micro-deformation to be as close as possible to the macroscopic plastic deformation, $\underset{\sim}{\boldsymbol{H}}^p$. In the limit, the use of a Lagrange multiplier instead of the penalty factor, H_χ, is necessary to enforce the internal constraint that

$$\underset{\sim}{\boldsymbol{\chi}}^p \equiv \underset{\sim}{\boldsymbol{H}}^p \tag{103}$$

In that case, the power of the internal forces, Eq. (91), coincides with that defined in Eq. (53). As a result, the *microcurl* model degenerates into the curl $\underset{\sim}{\boldsymbol{H}}^p$ theory described in Section 3. In Eringen's and Mindlin's micromorphic theory, the micro-deformation can be constrained to be as close as possible to the macrodeformation, represented by the usual deformation gradient tensor. Then, the micromorphic model reduces to Mindlin's second gradient theory. We adopt here a similar constraint such that the *microcurl* model degenerates into Gurtin's strain gradient plasticity model. The curl of micro-deformation $\underset{\sim}{\boldsymbol{\Gamma}}_\chi$ coincides with the dislocation density tensor only when this constraint is enforced. This suggests that, in the general unconstrained case, the micro-deformation $\underset{\sim}{\boldsymbol{\chi}}^p$ should not depart too much from the plastic deformation for the $\underset{\sim}{\boldsymbol{\Gamma}}_\chi$ measure to still have the physical meaning of a quantity close to the dislocation density tensor. The departure of the micro-deformation from the plastic deformation introduces a new constitutive ingredient in the model that remains however of a purely phenomenological nature. This constitutive law, embodied by the additional parameter H_χ, is shown in what follows to lead to more general scaling laws than the original strain gradient plasticity model.

The micromorphic model can also be seen as a regularisation of the curl $\underset{\sim}{\boldsymbol{H}}^p$ theory which displays some discontinuity at the interface between the elastic and the elasto-plastic zones. Another way of solving the indeterminacy problem is to track the limit of the elastic domain and to enforce an *a priori* condition of vanishing double traction (Liebe et al., 2003) on this surface. However, with such conditions, it has been shown that the laminate boundary value problem of interest does not admit any non-trivial solution.

4.4. Application to a two-phase periodic microstructure under simple shear

Contrary to the curl $\underset{\sim}{\boldsymbol{H}}^p$ theory, plastic micro-deformation can develop even in the absence of macroscopic plastic strain. In particular, double stresses that may arise in a plastic phase can be transmitted to an elastic phase through the interface.

Let us consider again the two-phase microstructure under simple shear of Section 3 and apply the *microcurl* model to that problem. We consider a slip system whose slip direction is along the axis 1, i.e., the shear direction in Fig. 2. The unknowns of the problems are one component of the displacement vector and two components of the plastic micro-deformation tensor, namely,

$$u_1 = \overline{\gamma} x_2, \quad u_2(x_1), \quad u_3 = 0, \quad \chi^p_{12}(x_1), \quad \chi^p_{21}(x_1), \tag{104}$$

$$[\underset{\sim}{\boldsymbol{H}}] = \begin{bmatrix} 0 & \overline{\gamma} & 0 \\ u_{,1} & 0 & 0 \\ 0 & 0 & 0 \end{bmatrix}, \quad [\underset{\sim}{\boldsymbol{H}}^p] = \begin{bmatrix} 0 & \gamma & 0 \\ 0 & 0 & 0 \\ 0 & 0 & 0 \end{bmatrix}, \quad [\underset{\sim}{\boldsymbol{H}}^e] = \begin{bmatrix} 0 & \overline{\gamma}-\gamma & 0 \\ u_{2,1} & 0 & 0 \\ 0 & 0 & 0 \end{bmatrix}, \tag{105}$$

$$[\underset{\sim}{\boldsymbol{\chi}}^p]=\begin{bmatrix}0 & \chi^p_{12}(x_1) & 0\\ \chi^p_{21}(x_1) & 0 & 0\\ 0 & 0 & 0\end{bmatrix},\quad [\mathrm{curl}\,\underset{\sim}{\boldsymbol{\chi}}^p]=\begin{bmatrix}0 & 0 & -\chi^p_{12,1}\\ 0 & 0 & 0\\ 0 & 0 & 0\end{bmatrix}. \tag{106}$$

The resulting stress tensors are

$$[\underset{\sim}{\boldsymbol{\sigma}}]=\mu\begin{bmatrix}0 & \overline{\gamma}-\gamma+u_{2,1} & 0\\ \overline{\gamma}-\gamma+u_{2,1} & 0 & 0\\ 0 & 0 & 0\end{bmatrix},\quad [\underset{\sim}{\boldsymbol{s}}]=-H_\chi\begin{bmatrix}0 & \gamma-\chi^p_{12} & 0\\ -\chi^p_{21} & 0 & 0\\ 0 & 0 & 0\end{bmatrix}, \tag{107}$$

$$[\underset{\sim}{\boldsymbol{M}}]=\begin{bmatrix}0 & 0 & -A\chi^p_{12,1}\\ 0 & 0 & 0\\ 0 & 0 & 0\end{bmatrix},\quad [\mathrm{curl}\,\underset{\sim}{\boldsymbol{M}}]=\begin{bmatrix}0 & -A\chi^p_{12,11} & 0\\ 0 & 0 & 0\\ 0 & 0 & 0\end{bmatrix}. \tag{108}$$

The balance equation, $\underset{\sim}{\boldsymbol{s}}=-\mathrm{curl}\,\underset{\sim}{\boldsymbol{M}}$, gives

$$\chi^p_{21}=0,\quad H_\chi(\gamma-\chi^p_{12})=-A\chi^p_{12,11}. \tag{109}$$

Furthermore, the plasticity criterion stipulates that

$$\sigma_{12}+s_{12}=\sigma_{12}+A\chi^p_{12,11}=\tau_c. \tag{110}$$

The force stress balance equation requires that σ_{12} be constant. It follows that

$$\chi^p_{12,111}=0, \tag{111}$$

and the plastic micro-deformation profile in the soft phase is therefore parabolic:

$$\chi^{ps}_{12}=a^s x_1^2+c, \tag{112}$$

where symmetry conditions have already been taken into account ($\chi^{ps}_{12}(-s/2)=\chi^{ps}_{12}(s/2)$), and a^s and c are constants to be determined. The plastic slip can be computed from Eq. (109). In the elastic domain, the balance equation (109) is still valid with vanishing plastic slip so that the profile of plastic micro-deformation is hyperbolic:

$$\chi^{ph}_{12}=a^h\cosh\left(\omega^h\left(x_1-\frac{s+h}{2}\right)\right)\quad\text{with }\omega^h=\sqrt{\frac{H^h_\chi}{A^h}}, \tag{113}$$

for $s/2\le|x_1|\le(s+h)/2$. Note that symmetry conditions have already been taken into account ($\chi^{ph}_{12}(s/2)=\chi^{ph}_{12}(s/2+h)$). The identification of the coefficients, a^h, a^s, c, is possible by means of the following interface and periodicity conditions:

- Continuity of χ^p_{12} at $x_1 = s/2$:

$$a^s\left(\frac{s}{2}\right)^2+c=a^h\cosh\frac{\omega^h h}{2}. \tag{114}$$

  The periodicity condition for χ^p_{12} at $x_1=-s/2$ and $x_1 = s/2+h$ leads to the same equation.
- Continuity of the double traction $m_{12} = -M_{13}$ at $x_1 = s/2$, according to Eq. (93):

$$M^h_{13}=-A^h\chi^{ph}_{12,1}=-a^hA^h\omega^h\sinh\left(x_1-\frac{s+h}{2}\right)=M^s_{13}=-A^s\chi^{ps}_{12,1}=-2a^sA^sx_1. \tag{115}$$

  so that

$$2A^sa^s\frac{s}{2}=-A^ha^h\omega^h\sinh\frac{\omega^h h}{2}. \tag{116}$$

  Likewise, the periodicity condition for M_{13} at $x_1=-s/2$ and $x_1 = (s/2+h)$ leads to the same equation as above.
- The plasticity condition in the soft phase provides the value of the constant stress component:

$$\sigma_{12}=\tau_c-2A^sa^s. \tag{117}$$

- Consequence of the periodicity of the displacement component u_2. We start from

$$\sigma_{12}=\mu(\overline{\gamma}-\gamma+u_{2,1})\implies u^s_{2,1}=\frac{\sigma_{12}}{\mu}+\gamma-\overline{\gamma}, \tag{118}$$

  so that

$$u^s_{2,1}=\frac{\sigma_{12}}{\mu}-\overline{\gamma}+a^sx_1^2+c-\frac{2A^sa^s}{H^s_\chi} \tag{119}$$

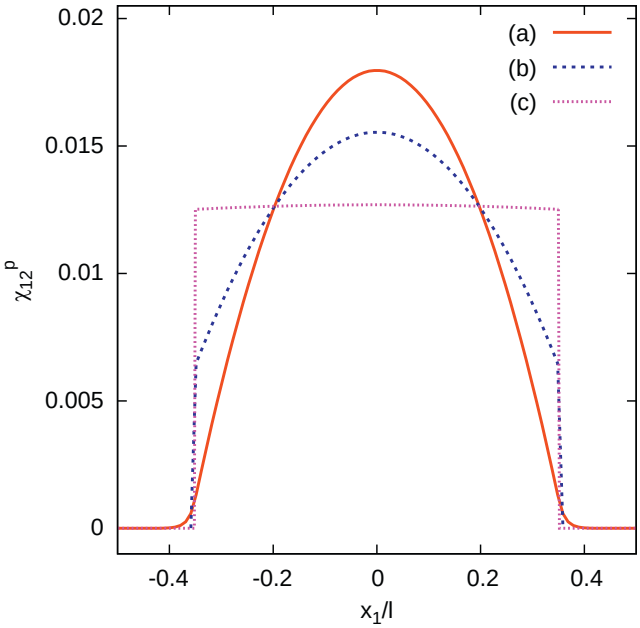

Fig. 4. Profiles of plastic micro-deformation χ_{12}^p in the two-phase microstructure with the *microcurl* model: (a) obtained with a set of material parameters to visualise the smooth transition at the elasto-plastic interface ($\mu = 35\,000$ MPa, $H_\chi^h = H_\chi^s = 133\,829$ MPa, $A^h = A^s = 2\times10^{-5}$ MPa mm^2 and $\tau_c = 40$ MPa); (b) with a stronger mismatch between the moduli of the two phases $A^h = 2\times10^{-7}$ MPa mm^2 and $A^s = 2\times10^{-5}$ MPa and (c) $A^h = 2\times10^{-11}$ MPa mm^2 and $A^s = 2\times10^{-5}$ MPa mm^2, which leads to sharper profiles at the interfaces. In all three cases, $f_s = 0.7$ and the $A^{h,s}$ values are chosen for $l = 1$ μm.

in the plastic phase. In contrast, in the elastic phase, we have

$$u_{2,1}^h = \frac{\sigma_{12}}{\mu} - \overline{\gamma}. \tag{120}$$

We compute the average:

$$\int_{-s/2}^{s/2+h} u_{2,1}\, dx_1 = 0, \tag{121}$$

which vanishes for periodicity reasons and gives

$$\left(\frac{\sigma_{12}}{\mu} - \overline{\gamma}\right)(s+h) + \left(c - \frac{2A^s a^s}{H_\chi^s}\right)s + \frac{2}{3}a^s\left(\frac{s}{2}\right)^3 = 0. \tag{122}$$

The solutions of Eqs. (114)–(122) are

$$a^s = (s+h)\left(\overline{\gamma} - \frac{\tau_c}{\mu}\right)\left(-\frac{2A^s}{\mu}(s+h) - \left(\left(\frac{s}{2}\right)^2 + \frac{sA^s}{\omega^h A^h}\coth\frac{\omega^h h}{2}\right)s - \frac{2A^s s}{H_\chi^s} + \frac{2}{3}\left(\frac{s}{2}\right)^3\right)^{-1}, \tag{123}$$

$$a^h = -\frac{1}{\sinh\frac{\omega^h h}{2}}\frac{sA^s}{\omega^h A^h}a^s, \tag{124}$$

$$c = -\left(\left(\frac{s}{2}\right)^2 + \frac{sA^s}{\omega^h A^h}\coth\frac{\omega^h h}{2}\right)a^s. \tag{125}$$

The corresponding profiles of plastic micro-deformation are illustrated in Fig. 4 for three different sets of material parameters. The first parameters are chosen to clearly visualise the parabolic profile in the soft phase and the hyperbolic profiles in the elastic phase. When $A^s = A^h$, the slope of the plastic micro-deformation is continuous at the interface, as can be seen in Fig. 4(a). The two other sets of material parameters introduce a stronger mismatch between the moduli A^h and A^s. Accordingly, the micro-variable χ^p decreases rapidly in the elastic phase, while it is still continuous at the interface. The profile of Fig. 4(c) is almost flat. In all cases, the coupling modulus has been taken high enough so as the plastic micro-deformation almost coincides with the plastic slip in the soft phase.

5. Overall size effects predicted by the Cosserat, *microcurl* and "*curl H^p*" models

Based on the non-homogeneous distribution of mechanical variables in a two-phase laminate undergoing simple shear as determined for the Cosserat and the *microcurl* models, see Sections 2.2 and 4.4, we now study more specifically the macroscopic response of the laminate and the macroscopic size effects predicted by the two models. Due to the similarity of the models, their responses are analysed in parallel. Differences however exist and will be pointed out. This section is organised as follows. First, the macroscopic stress strain curve is calculated for the laminate material. The overall hardening moduli are also determined. The second subsection analyses the predicted size effects. For simplicity, we assume here that the shear moduli of the two phases are equal: $\mu_s = \mu_h = \mu$.

5.1. Predicted macroscopic stress–strain response and kinematic hardening modulus

When deriving the overall properties of a periodic generalised medium, the development of specific homogenisation tools are required. Such methods were developed for heterogeneous strain gradient and Cosserat media in Smyshlyaev and Fleck (1996) and Forest et al. (2001), respectively. The effective material is regarded here as a classical Cauchy material endowed with effective elasto-plastic properties. We derive the expression of the macroscopic Cauchy stress tensor component, Σ_{12}, defined as the mean value of the stress component σ_{12} over the unit cell of size $l=(s+h)$:

$$\Sigma_{12} = \langle \sigma_{12} \rangle = \frac{1}{l}\int_{-l/2}^{l/2} \sigma_{12}\, dx_1. \tag{126}$$

Note that for the Cosserat model, the local stress tensor is non-symmetric, even though for the simple shear boundary value problem considered here, we find that the average stress component $\langle \sigma_{12} \rangle = \langle \sigma_{21} \rangle = \Sigma_{12}$. Expressions for the local stress σ_{12} were derived in Sections 2.2 and 4.4, in terms of the coefficients (a^s, d^s, a^h, d^h). The following form can be adopted for the coefficient, a^s, which is valid for both the Cosserat and the *microcurl* models,

$$a^s = \frac{\mathcal{A}}{\mathcal{B}l^2 + \mathcal{C}l\coth\left(\omega^h \frac{l(1-f_s)}{2}\right) + \mathcal{D}}, \tag{127}$$

Table 1 gives the values of $\mathcal{A}$, $\mathcal{B}$, $\mathcal{C}$, $\mathcal{D}$ introduced in Eq. (127) for both models. An equivalence can be found between Cosserat and *microcurl* material parameters, which is valid for the boundary value problem of interest here

$$A \equiv 2\beta, \tag{128}$$

$$H_\chi \equiv 4\frac{\mu\mu_c}{\mu+\mu_c}. \tag{129}$$

However, identification of μ_c for a given value of H_χ is not always possible due to the non-linear relation, Eq. (129), that allows only values of H_χ smaller than

$$\lim_{\mu_c\to\infty} 4\frac{\mu\mu_c}{\mu+\mu_c} = 4\mu \tag{130}$$

Next, results are presented for the *microcurl* model. The corresponding expressions for the Cosserat model can be obtained using the previous equivalence relations. The macroscopic stress component, Σ_{12}, can be obtained knowing the applied shear strain, $\overline{\gamma}$, and mean plastic slip, $\langle \gamma \rangle$. Recalling Eq. (117),

$$\Sigma_{12} = \frac{1}{s+h}\int_{-l/2}^{l/2} \sigma_{12}\, dx_1 = \tau_c - 2A^s a^s = \mu(\overline{\gamma} - \langle \gamma \rangle / f_s). \tag{131}$$

Table 1
Coefficients needed to determine the integration constant a^s from Eq. (127), as a function of the applied shear strain $\overline{\gamma}$ for both the Cosserat and *microcurl* models.

	Model	Cosserat	*microcurl*
$a^s(\overline{\gamma})$	$\mathcal{A}$	$\frac{\tau_c}{\mu} - \overline{\gamma}$	$\frac{\tau_c}{\mu} - \overline{\gamma}$
	$\mathcal{B}$	$\frac{f_s^3}{6}$	$\frac{f_s^3}{6}$
	$\mathcal{C}$	$\frac{f_s^2 \beta^s}{\beta^h \omega^h}$	$\frac{f_s^2 A^s}{A^h \omega^h}$
	$\mathcal{D}$	$\beta^s\left(f_s\frac{\mu+\mu_c}{\mu\mu_c} + \frac{4}{\mu}\right)$	$A^s\left(\frac{2f_s}{H_\chi^s} + \frac{2}{\mu}\right)$

The mean plastic slip is determined from Eq. (109) as follows:

$$\langle\gamma\rangle=\left\langle\chi^p_{12}-\frac{A^s}{H^s_\chi}\chi^p_{12,11}\right\rangle=\frac{1}{l}\int_{-s/2}^{s/2}\left(a^s\left(x_1^2-\frac{2A^s}{H^s_\chi}\right)+c\right)dx_1=\frac{1}{l}\left(a^s\frac{s^3}{12}+s\left(c-\frac{2A^sa^s}{H^s_\chi}\right)\right). \tag{132}$$

Accordingly, an alternative expression of a^s as a function of mean plastic strain is obtained:

$$a^s=\frac{\mathcal{A}'}{\mathcal{B}'l^2+\mathcal{C}'l\coth\left(\omega^h\frac{l(1-f_s)}{2}\right)+\mathcal{D}'}, \tag{133}$$

where coefficients $\mathcal{A}'$, $\mathcal{B}'$, $\mathcal{C}'$, $\mathcal{D}'$ are given in Table 2 for both the *microcurl* and Cosserat models. The predicted macroscopic stress–strain curve, for a microstructural length scale of size $l=s+h=10^{-3}$ mm, and the material parameters from Table 3, is shown in Fig. 5. To obtain the curves of Fig. 5, the laminate microstructure of Fig. 2 has been subjected to cyclic

Table 2
Coefficients needed to determine the integration constant a^s from Eq. (133), as a function of the mean plastic deformation, $\langle\gamma\rangle$, for both the Cosserat and *microcurl* models.

	Model	Cosserat	*microcurl*
$a^s(\langle\gamma\rangle)$	$\mathcal{A}'$	$-\langle\gamma\rangle$	$-\langle\gamma\rangle$
	$\mathcal{B}'$	$\frac{f_s^3}{6}$	$\frac{f_s^3}{6}$
	$\mathcal{C}'$	$\frac{f_s^2\beta^s}{\beta^h\omega^h}$	$\frac{f_s^2A^s}{A^h\omega^h}$
	$\mathcal{D}'$	$f_s\beta^s\frac{\mu+\mu_c}{\mu\mu_c}$	$\frac{2f_sA^s}{H^s_\chi}$

Table 3
Set of material parameters satisfying the equivalence conditions (128) and (129) between the *microcurl* and the Cosserat models.

Coefficient	μ (MPa)	τ_c (MPa)	Cosserat μ_c (MPa)	*microcurl* H_χ (MPa)	Cosserat β (MPa mm^2)	*microcurl* A (MPa mm^2)
Phase (s)	35 000	40	10^6	133 829	10^{-2}	2×10^{-2}
Phase (h)	35 000	–	10^6	133 829	10^{-5}	2×10^{-5}

The intrinsic length scales, defined as $\sqrt{A/H_\chi}$ or $\sqrt{\beta/\mu}$, induced by these parameters are of the order of 10 nm for the elastic phase (h) and 500 nm for the plastic phase (s).

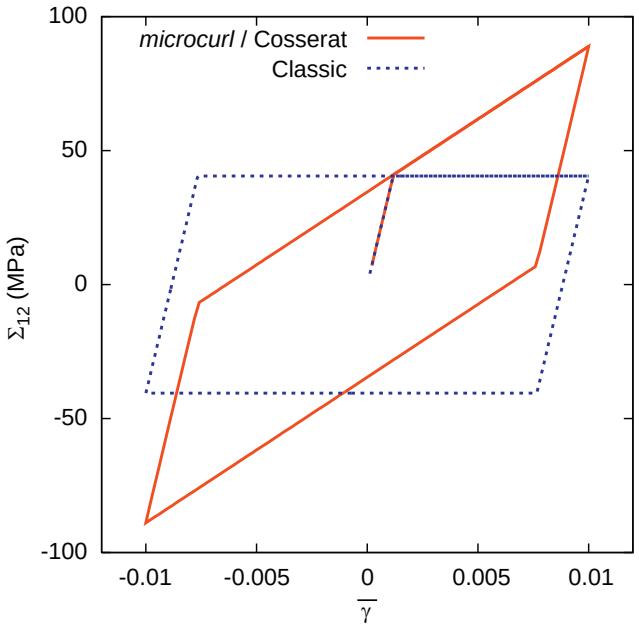

Fig. 5. Macroscopic stress–strain response of the laminate microstructure under cyclic shear loading conditions: comparison between the kinematic hardening predicted by both the *microcurl* and Cosserat models in comparison and the behaviour from a conventional crystal plasticity theory for $l=10^{-3}$ mm (the material parameters used are given in Table 3).

shear loading, controlled by the mean shear deformation $\overline{\gamma}$. The average stress component Σ_{12} has been then computed. The predicted response clearly exhibits pure linear kinematic hardening, in contrast to that obtained with the perfectly plastic classical crystal plasticity model that does not incorporate the higher order back stress component. Such kinematic hardening components are usually introduced directly into the constitutive equations of classical crystal plasticity, as done in Busso et al. (2000). The expression for the kinematic hardening modulus H can be obtained using Eqs. (131) and (133):

$$H = \frac{2A^s}{\mathcal{B}' l^2 + \mathcal{C}' l \coth\left(\omega^h \frac{l(1-f_s)}{2}\right) + \mathcal{D}'}. \tag{134}$$

This expression clearly shows that the hardening modulus is size-dependent for both the Cosserat and *microcurl* models. At the limit of vanishingly small microstructural size, l, for fixed intrinsic lengths of the generalised continua and fixed soft phase volume fraction, f_s, the following value of the hardening modulus is obtained:

$$\lim_{l\to 0} H = \frac{1-f_s}{\frac{f_s^2}{H_\chi^h} + \frac{f_s(1-f_s)}{H_\chi^s}}. \tag{135}$$

In the specific case when $H_\chi^h = H_\chi^s = H_\chi$, the limit becomes

$$\lim_{l\to 0} H = \frac{1-f_s}{f_s} H_\chi \tag{136}$$

for the *microcurl*, and

$$\lim_{l\to 0} H = \frac{1-f_s}{f_s} \frac{4\mu\mu_c}{\mu+\mu_c}. \tag{137}$$

for Cosserat. Eqs. (136) and (137) reveal a major difference between the two models. In the *microcurl* model, the limiting hardening modulus depends only on the parameter H_χ, whereas Cosserat depends on both the classical shear modulus, μ, and the Cosserat coupling modulus, μ_c. Moreover, taking into account the condition $\mu \ll \mu_c$ chosen for the Cosserat continuum, see Eq. (19), we find that, in that case, the limit hardening modulus saturates at

$$\lim_{l\to 0} H = \frac{1-f_s}{f_s} 4\mu. \tag{138}$$

In contrast, the kinematic hardening modulus in the *microcurl model* linearly increases with the coupling modulus H_χ.

The existence of such a back stress contribution from the dislocation density tensor was anticipated by Steinmann (1996), derived from statistical mechanical arguments by Groma et al. (2003) and simulated for a two-phase microstructure in Forest (2008). However, the previous analytical expressions of the hardening modulus were derived in none of these publications.

5.2. Predicted size-dependent macroscopic flow stress

The previous results make it possible to study the dependence of the flow stress at $\langle\gamma\rangle = 0.002$ as a function of the microstructural length scale $l=(s+h)$ for a given volume fraction of the soft phase, f_s. The overall flow stress is obtained by setting $\langle\gamma\rangle = 0.002$ in Eq. (131). Fig. 6 presents the predicted evolution of the flow stress as a function of l in a log–log diagram using the numerical values from Table 3 and for different values of the coupling modulus, $H_\chi^h = H_\chi^s = H_\chi$. All other material parameters are kept fixed, in particular, the intrinsic lengths associated with the moduli A^s and A^h (resp. β^s,β^h), which are assumed to be independent of l. The two lower curves in Fig. 6 are obtained for values of the coupling moduli lying in the range of equivalence between the Cosserat and *microcurl* models (i.e. satisfying the equivalence condition (129)). The dotted curve, obtained with $\mu_c = \infty$, shows the upper limit reached by the Cosserat model. The curves above are obtained for higher values of the coupling modulus H_χ.

For finite values of the coupling modulus, the curves exhibit a typical *tanh*- shape with a saturation for large ($l > 10^{-2}$ mm for the chosen parameters) and small ($l < 10^{-6}$ mm) values of l. Between these two asymptotic regimes, there is a transition domain for which significant size dependence is observed. This zone is situated between approximately $l=10^{-5}$ and 10^{-3} mm. The asymptotic values, the width of the transition zone, and the scaling law exponent in the transition regime are directly related to the material parameters used in both the Cosserat and *microcurl* models. The main characteristics of the *tanh*-curves are analysed in the two following subsections.

5.2.1. Asymptotic regimes and maximal size effect predicted by the models

When the size of the elasto-plastic phase becomes large compared to the intrinsic model material length scale, l_ω, strain gradients are small and the kinematic hardening contribution to the overall stress tends to vanish. In such case, the models reduce to classical crystal plasticity theory. The 0.2% macroscopic flow stress then evolves towards the critical resolved shear stress:

$$\lim_{l\to\infty} \Sigma_{12|0.2} = \tau_c. \tag{139}$$

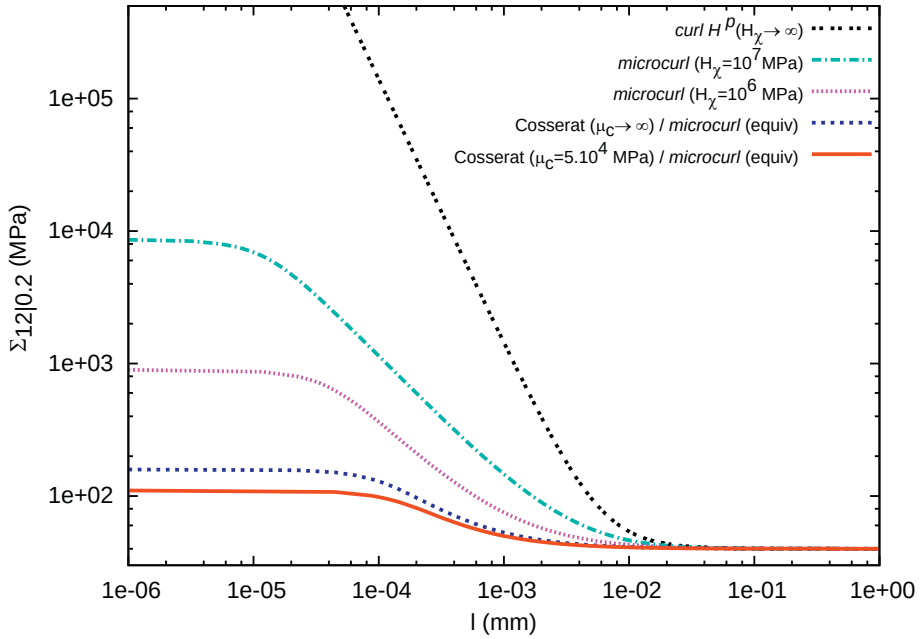

Fig. 6. Evolution of the macroscopic flow stress $\Sigma_{12|0.2}$ at 0.2% plastic strain as a function of the microstructure length scale l, plotted for different coupling moduli H_χ and μ_c of the Cosserat and *microcurl* models respectively.

In contrast, for small microstructure sizes, l, compared to the intrinsic material length scale, l_ω, the strain gradient effects dominate. The maximum size effect generated by the *microcurl* model is obtained for sizes lower than a critical value. For smaller and smaller microstructures, the stress at a given mean plastic strain $\langle\gamma\rangle$ saturates at

$$\lim_{l\to 0}\Sigma_{12}(\langle\gamma\rangle)=\tau_c+\frac{1-f_s}{f_s}\frac{H_\chi^h H_\chi^s\langle\gamma\rangle}{H_\chi^h(1-f_s)+H_\chi^s f_s}. \tag{140}$$

If the two coupling moduli are assumed equal, $H_\chi=H_\chi^s=H_\chi^h$, this limit becomes

$$\lim_{l\to 0}\Sigma_{12}(\langle\gamma\rangle)=\tau_c+\frac{1-f_s}{f_s}H_\chi\langle\gamma\rangle. \tag{141}$$

As a result, for a fixed $\langle\gamma\rangle$ value, there exists a maximum extra-stress $\Delta\Sigma$ induced by strain gradient effects according to the *microcurl* model:

$$\Delta\Sigma=\lim_{l\to 0}\Sigma_{12}(\langle\gamma\rangle)-\tau_c=\frac{1-f_s}{f_s}H_\chi\langle\gamma\rangle. \tag{142}$$

The maximum macroscopic extra-stress reachable by the model depends on the volume fraction, f_s, the mean plastic slip, $\langle\gamma\rangle$, and the coupling modulus, H_χ. Note that, for f_s and $\langle\gamma\rangle$ fixed, we can compute the following limit:

$$\lim_{H_\chi\to\infty}\left(\lim_{l\to 0}\Sigma_{12}\right)=\infty. \tag{143}$$

A similar expression for the maximum extra-stress predicted by the Cosserat model is

$$\Delta\Sigma=\frac{1-f_s}{f_s}\frac{4\mu\mu_c}{\mu+\mu_c}\langle\gamma\rangle \tag{144}$$

which, when μ_c goes to infinity, tends to

$$\Delta\Sigma^\infty=\frac{1-f_s}{f_s}4\mu\langle\gamma\rangle. \tag{145}$$

This expression clearly shows that the maximal size effect predicted by the Cosserat model is bounded, in contrast to that predicted by the *microcurl* model. Consequently, as noted in the previous subsection about the hardening modulus, the Cosserat and *microcurl* models behave differently for small values of l. The Cosserat maximum size effect is intrinsically limited by the elastic properties for a given fraction of the phase (s), whereas the maximum size effect predicted by the *microcurl* model is entirely controlled by the H_χ coefficient.

These different responses are illustrated by Fig. 7, where the extra-stress at 0.2% plastic strain is plotted as a function of the coupling modulus for the two models. As it was shown in Section 5.1 and in Fig. 6, the two models considered here are equivalent for sufficiently small values of the coupling modulus, according to the expression (129).

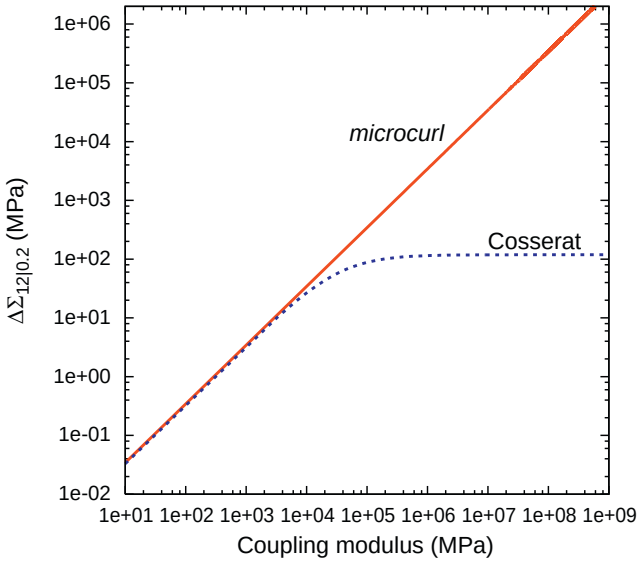

Fig. 7. Evolution of the 0.2% macroscopic flow stress, $\Delta\Sigma_{12|0.2}$, as a function of the coupling modulus for the Cosserat and *microcurl* models. The abscissa corresponds to H_χ for the *microcurl* model and to $4\mu_c$ for the Cosserat model (first order Taylor approximation of Eq. (129) for μ_c near zero). The material parameters considered for each phase are given in Table 3.

5.2.2. *Predicted transition zone and scaling law*

The transition domain between the size-independent and dependent flow stress can be characterised by two main parameters, see Fig. 1. A critical value of l, denoted l_c, is defined as the inflection point of the $\log l - \log\Sigma_{0.2}$ curve. The inflection point l_c can be computed, for instance, for all the curves of Fig. 6. Moreover, the scaling law, of the form l^n, is defined by the first derivative of the curve, $\log l - \log\Sigma_{0.2}$ at $l=l_c$. The values l_c and n are determined numerically. For the material parameters given in Table 3, we found $l_c \simeq 2.24 \times 10^{-5}$ mm and the slope at this point is $n \simeq -0.46$.

Next, we present the model predictions of the evolution of l_c as a function of the material parameters. For a fixed modulus, $A^s = 10^{-1}$ MPa mm^2, the microstructure size dependence of the flow stress is plotted in Fig. 8(a) for different values of A^h. The other parameters are taken equal to their values in Table 3. These curves show that the transition zone is translated towards smaller microstructural length scales when A^h is decreased. Similar results hold for the $\beta^{h,s}$ values in the Cosserat model. For a fixed modulus $A^h = 10^{-1}$ MPa mm^2, the microstructural length scale dependence of the flow stress is plotted in Fig. 8(b) for different values of A^s. The translation of the transition zone is still observed.

From these curves, the characteristic length scale, l_c, and the scaling law exponent, n, can be determined and plotted as functions of A^h and A^s, see Fig. 9. The characteristic length l_c increases with $A^{s,h}$, and eventually saturates. For the chosen parameters, the scaling power law remains close to $n=-0.5$. The values of l_c and n also depend on that of the coupling modulus. Fig. 10(a) gives the dependence of the inflection point of the curves of Fig. 6 with respect to the values of the coupling moduli μ_c and H_χ, for fixed values of the remaining parameters, especially $A^{h,s}$ which describe the gradient effect. The predictions of the *microcurl* model shown in Fig. 10 are obtained analytically. A bump is observed on the l_c curve for the *microcurl* model. It seems to be the result of two competing effects of material parameters. On the one hand, increasing H_c leads to a translation of the inflection point to the left in Fig. 6. When $H_\chi \to \infty$, there is no longer an inflection point, this is the reason why the red curve converges toward zero for large values of the coupling modulus. On the other hand, increasing H_χ leads to an increase in the slope of the quasi-linear part of the $\log\Sigma_{0.2} = f(\log l)$ curve, which in turn tends to slightly move the inflection point to the right in Fig. 6. We find that there exists a domain of H_χ values for which the second effect becomes dominant. This non-linear effect remains limited. Probably, there exists a combination of parameters H_χ and A that would lead to a monotonic decrease of l_c. Fig. 10(b) shows that the coupling modulus has a major effect on the scaling law for both models. In contrast, it has a limited effect on the size-dependent region location since it is generally taken around an equivalent value of 10^6 MPa. It turns out that, for the chosen material parameters, the Cosserat model provides power law exponent values that saturate close to $n=-0.5$ in the highly constrained case. In contrast, the asymptotic power law for the *microcurl* model is close to $n=-2$.Indeed, when the coupling modulus H_χ tends to infinity, we can derive an asymptotic expression for a^s. In Eq. (133), the $\mathcal{C}'$ and $\mathcal{D}'$ coefficients tend to zero and the coth function tends toward 1. In that specific case, the flow stress becomes

$$\lim_{H_\chi \to \infty} \Sigma_{12} = \tau_c + \frac{12A^s \langle \gamma \rangle}{f_s^3 l^2}. \tag{146}$$

This expression indicates an $n=-2$ scaling law. Fig. 11 presents the effect of the volume fraction f_s on the scaling law for the constrained Cosserat and *microcurl* models, i.e., for high values of the coupling moduli, μ_c and H_χ, respectively. According to the *microcurl* model, f_s has no effect on the asymptotic power law exponent of $n=-2$. For the Cosserat model, the effect of volume fraction is strong and dominates when the coupling modulus μ_c is high. The range of reachable scaling laws lies

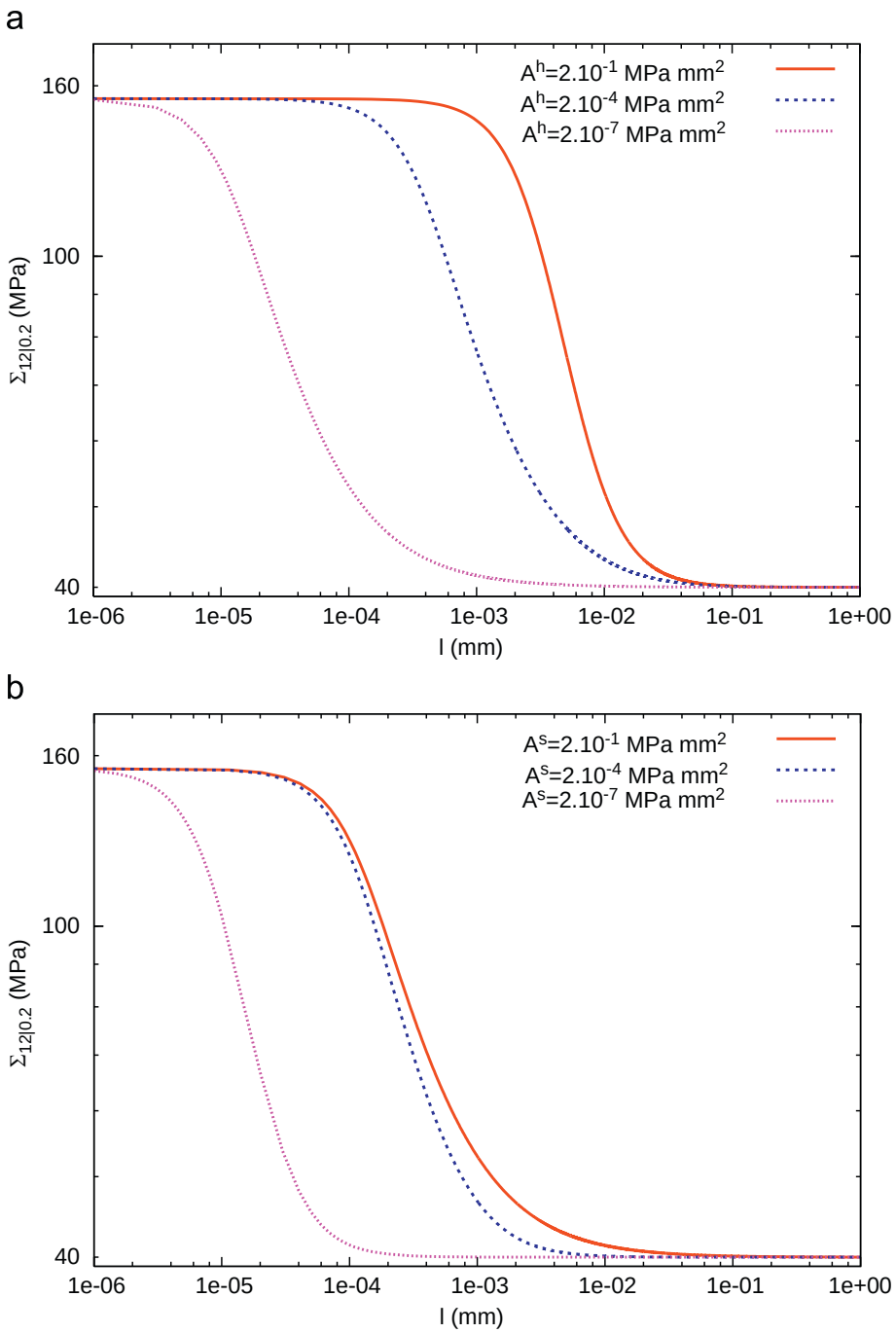

Fig. 8. Effect of the higher order moduli A^h and A^s on the evolution of the macroscopic 0.2% flow stress $\Sigma_{12|0.2}$, as a function of the microstructural length scale l for: (a) different values of A^h (or β^h), and A^s=10^{-1} MPa mm^2; (b) different values of A^s (or β^s), and A^h=10^{-1} MPa mm^2.

between 0 and -1. The -1 scaling law is obtained when the fraction of the soft phase tends to 0, i.e., when the microstructure is mainly constituted by hard obstacles. In this case, the Cosserat model delivers the same scaling law as the Orowan effect for precipitate hardening:

$$\Sigma_{12}-\tau_c \propto \frac{1}{l} \tag{147}$$

An approximation of the flow stress can be derived when f_s tends to 0. In the transition zone we have checked that the coth term in Eq. (133) is close to 1. Consequently,

$$\lim_{f_s\to 0}\Sigma_{12}=\tau_c+\beta^s\frac{\mathcal{A}'}{\mathcal{C}'l+\mathcal{D}'}. \tag{148}$$

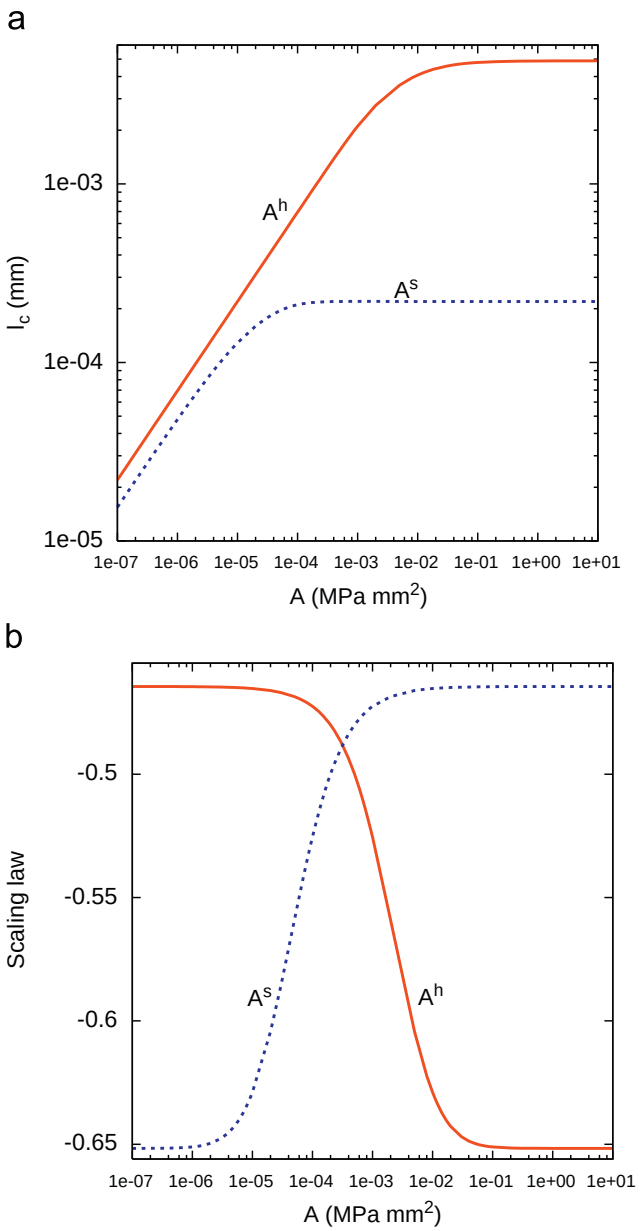

Fig. 9. Effect of the higher order moduli A^h and A^s on (a) the location l_c of the size-dependent region, and (b) the scaling power law exponent n. These evolutions are plotted as functions of one higher order modulus (A^h or A^s) while the other one is fixed.

This expression can be simplified considering that μ_c goes to ∞:

$$\lim_{f_s\to 0}\Sigma_{12}=\tau_c+\frac{\langle\gamma\rangle}{\frac{f_s^2}{\sqrt{2}}\frac{l_\omega l}{\beta^h}+\frac{f_s}{4\mu}}, \tag{149}$$

where l_ω is the characteristic length of the phase (h) defined by Eq. (18). Eq. (149) confirms the scaling law exponent of $n=-1$ predicted by the Cosserat model when f_s tends to 0.

The physical implications of these findings will be discussed in Section 6.

6. Discussion

The objective of this section is to discuss the previous results and to compare the pros and cons of the three models, namely the Cosserat, "*curl* H^p" and *microcurl*. In particular, we insist on the major importance of the interface conditions in the evaluation of the different approaches. As an illustration, it is shown that the explicit relations obtained for the main characteristics of the size-dependent model responses in the case of simple shear of a laminate, could be used for the identification of material parameters for a real two-phase material. Finally, the obtained results are proved to hold also in the case of a laminate microstructure endowed with two symmetric slip systems and undergoing simple shear.

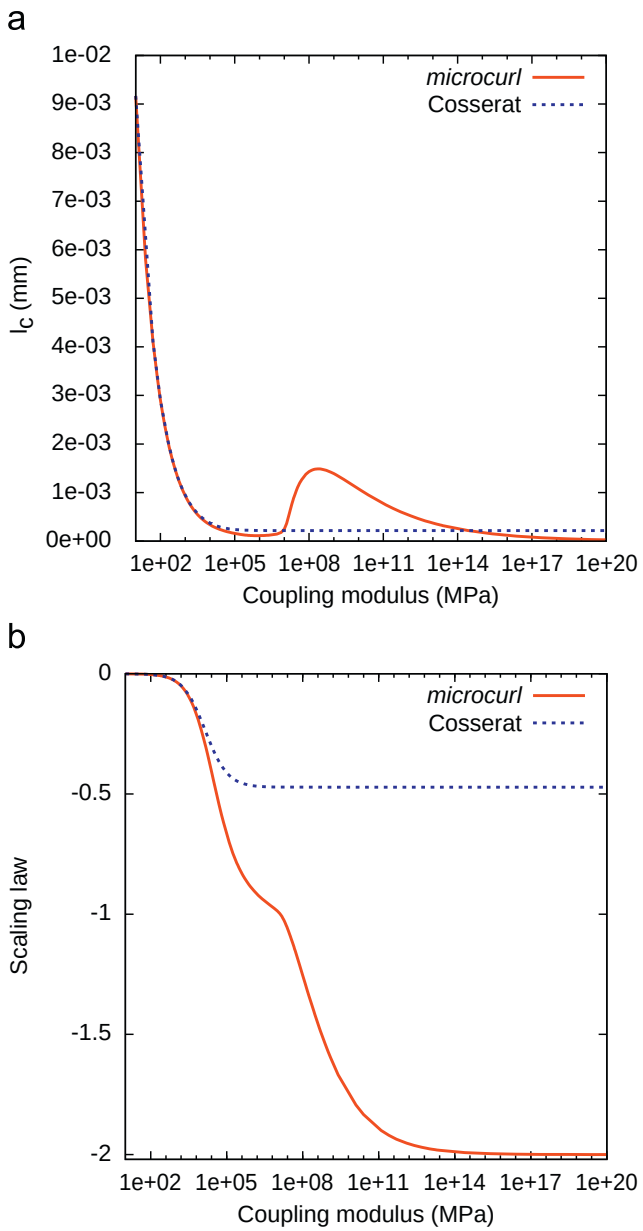

Fig. 10. Effect of the coupling moduli μ_c and H_χ on (a) the location l_c of the size-dependent transition zone, and (b) the scaling power law exponent n. The abscissa corresponds to H_χ for the *microcurl* model and to $4\mu_c$ for the Cosserat model (first order Taylor approximation of Eq. (129) when μ_c nears zero).

6.1. *Towards an identification of material parameters*

The main features of the scaling behaviour of Cosserat, micromorphic and strain gradient plasticity models have been quantitatively described in the special case of a two-phase laminate microstructure. Explicit formula or numerical estimates of the extra-hardening associated with plastic strain gradients, asymptotic behaviour and scaling laws have been provided for this specific case. A parametric study has shown that a large range of size effects can be explored depending on the higher order theories' material parameters. The previous analyses therefore set guidelines for the identification of such material parameters to describe specific size effects. Simple analytical situations like the one proposed in this work can help to estimate the order of magnitude of such parameters, see also Hunter and Koslowski (2008). The targeted phenomena are precipitate hardening and grain size effects. Generalisations of the approach will be necessary to tackle more realistic microstructures. This will also require intensive numerical simulations.

Depending on the amplitude and the range of observed size effects, the Cosserat and *microcurl* theories are suitable models to predict the size-dependent response of elasto-(visco)plastic crystalline solids. The Cosserat formulation has the particular advantage of requiring three additional degrees of freedom in contrast to the nine required by the micromorphic approach. However, it has been shown in Section 5.2.1 that the Cosserat crystal plasticity model may not be sufficient to account for large amplitude extra-hardening over a broad range of length scales, see Eq. (145).

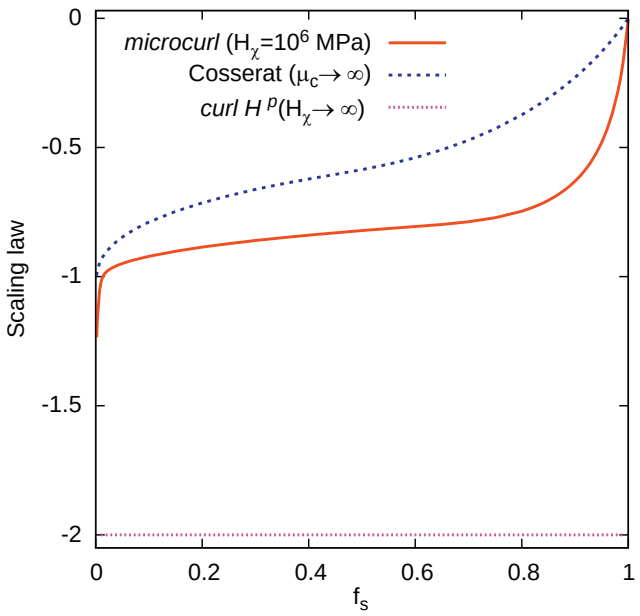

Fig. 11. Effect of the volume fraction f_s on the scaling law reachable by each model (obtained for high values of the coupling moduli).

Experimental results on size effects are generally available for a limited range of length scales. The transition domain between the two asymptotic regimes of the flow stress curve as a function of microstructure length scale, see Fig. 10, can therefore be calibrated in order to coincide with the measured experimental range. The existence of a saturated asymptotic regime below the experimentally investigated length scales, i.e., below l_c, can be seen as the limit of the continuum approach. That is why predictive extrapolations to smaller scales of the generalised continuum models should not be expected.

The power law exponent n of the Cosserat and *microcurl* models is not intrinsic to the form of the chosen constitutive equations but rather strongly depends on the values of the material parameters. It can be calibrated from experimental results in the range $-2 \leq n \leq 0$. These models can therefore be used to describe mixed Hall-Petch and Orowan effects. In contrast, the "*curl* H^p" model, regarded as the limiting case of the *microcurl* model for large values of H_χ, systematically leads to a power law exponent $n=-2$, which does not correspond to any known physical situation in crystal plasticity, to the best of our knowledge.

For the transmission of higher order tractions at the interface between elastic and elasto-plastic phases, it has been necessary to introduce higher order moduli like A^s and A^h in both phases. The absence of such transmission rules leads to a discontinuity of generalized tractions in the strict strain gradient plasticity theory. These higher order moduli can be seen as representing intrinsically non-local effects that work at different length scales. Non-local elasticity effects are expected at very low length scales, typically 10 nm, which motivates low values of the parameter A^h. In contrast, the volume element of a generalised crystal plasticity model must contain a sufficient number of dislocations for a continuum theory to apply. Non-local micro-plasticity effects occur at scales ranging typically from 0.3 to 10 μm in FCC metals. So we expect that $A^h \ll A^s$. These remarks set guidelines for the identification procedure and motivates the selected values of the material parameters in the examples provided in the previous sections (see Table 3).

As a formal exercise and with a view to setting guidelines for the identification of a more realistic model in the future, we propose in this section to calibrate the parameters $A^{h,s}$,H_χ, etc., of the *microcurl* (and Cosserat) models from experimental results for a material which shares some common features with the ideal laminate microstructures. Such experimental results in the form of precipitate size effects in single crystal nickel base superalloys can be found in Duhl (1987). Here, the microstructure consists of a quasi-periodic distribution of cuboidal γ' precipitates coherently embedded in the γ matrix. In a certain range of temperature and strain rate, the precipitates can be regarded as elastic whereas the matrix displays a complex elasto-viscoplastic behaviour. The narrow channels of γ phase are reminiscent of the ideal laminate microstructure of Fig. 2.

The precipitate size effect in such quasi-periodic microstructures has been modelled by means of periodic homogenisation techniques based on cubic unit cells, and using generalised continuum models by Busso et al. (2000), Forest et al. (2000) and more recently by Tinga et al. (2008). In the two first references, the size effect is entirely accounted for by the strain gradient approach, whereas the strain gradient plasticity model used by Tinga et al. (2008), also includes the Orowan law explicitly introduced in the constitutive model. In the context of the simple laminate model considered here, we will try to identify the higher order material parameters so as to describe the experimental precipitate hardening effect without including explicitly Orowan's law in the model. As it will be shown, the Orowan effect will arise naturally as a result of the generalised crystal plasticity formulation. This formal identification aims at discriminating the ability of the Cosserat and *microcurl* models to account for significant additional hardening due to strain gradient effects.

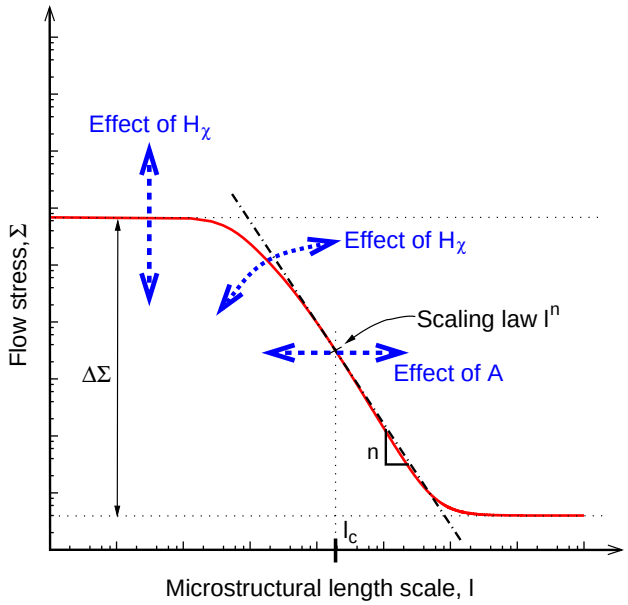

Fig. 12. Influence of each material parameter on the size effect predicted by the considered model.

The identification remains somehow idealised since we consider only single slip, which is not the dominant deformation mode in real superalloys. The slip geometry is also different from the reality, even though the soft phase of the laminate model mimics a γ- channel. Finally, the size effect observed in tension along the [0 0 1] crystallographic orientation is converted in terms of the resolved shear stress and slip amount, τ/γ, on one of the eight systems that are activated for this tensile test, see Fig. 13. Fig. 13 shows that the *microcurl* model is able to simulate an Orowan-like scaling law, that is when $n\sim-1$. Moreover, the identified characteristic length, l_c=200 nm, is approximately the matrix channels width in Ni-base superalloys. The calibrated parameters are given in the caption of Fig. 13. For an unambiguous identification, we have adopted $H^s_\chi = H^h_\chi = H_\chi$. This leaves three parameters that have been identified in order to account for the three characteristics of the size effect, namely $\Delta\Sigma$, l_c and n, see Fig. 12. The experimental results are available only over a narrow window of precipitate sizes, from 0.2 to 2 μm, so that the calibration of the three parameters leads to correct description of the experimental curve. The predicted ratio, $A^s/A^h \approx 10$, confirms the difference in characteristic lengths for the elastic and plastic phases. The relatively high value found for A^h shows the important role of the double traction transfer at the interface. The identified value of the parameter H_χ is such that an equivalence with the Cosserat model is possible. As a result, both the Cosserat and *microcurl* models are suitable to describe the superalloy behaviour. More detailed comparisons with experiment would be necessary to further study both approaches.

6.2. Extension to double slip

The Cosserat and *microcurl* models have common features with the statistical model of dislocations developed for single slip by Groma et al. (2003) as well as with results obtained from discrete dislocation dynamics simulations in Yefimov et al. (2004). The strain gradient plasticity model used in the two latter references has been extended for multiple slip situations using purely phenomenological arguments in Yefimov and Van der Giessen (2005) and Bardella (2007). In the same way, the Cosserat and *microcurl* models possess a straightforward phenomenological generalisation for multiple slip, without introducing neither additional ingredients nor parameters, but without confirmation that it is indeed consistent with the actual multislip behaviour of crystals. This formulation is illustrated for symmetric double slip in the laminate microstructure under shear loading conditions. Two slip systems, symmetric with respect to direction 1 and inclined at an angle $\pm\theta$ with respect to direction 1 are taken into account in the soft phase (s), as shown in Fig. 14. The main unknowns remain the same as in Section 4.4, see Eq. (104). Following the same procedure as in the case of single slip, one obtains

$$[\underset{\sim}{\boldsymbol{H}}] = \begin{bmatrix} 0 & \overline{\gamma} & 0 \\ u_{2,1} & 0 & 0 \\ 0 & 0 & 0 \end{bmatrix}, \quad [\underset{\sim}{\boldsymbol{H}}^p] = \begin{bmatrix} 0 & H^p_{12} & 0 \\ H^p_{21} & 0 & 0 \\ 0 & 0 & 0 \end{bmatrix}, \quad [\underset{\sim}{\boldsymbol{H}}^e] = \begin{bmatrix} 0 & \overline{\gamma}-H^p_{12} & 0 \\ u_{2,1}-H^p_{21} & 0 & 0 \\ 0 & 0 & 0 \end{bmatrix}. \tag{150}$$

As the two slip systems are symmetric, the associated plastic slips are equal $\gamma^1 = \gamma^2 = \gamma$. Then the non-zero components of the plastic deformation are

$$H^p_{12} = 2\gamma\cos^2\theta, \quad H^p_{21} = -2\gamma\sin^2\theta. \tag{151}$$

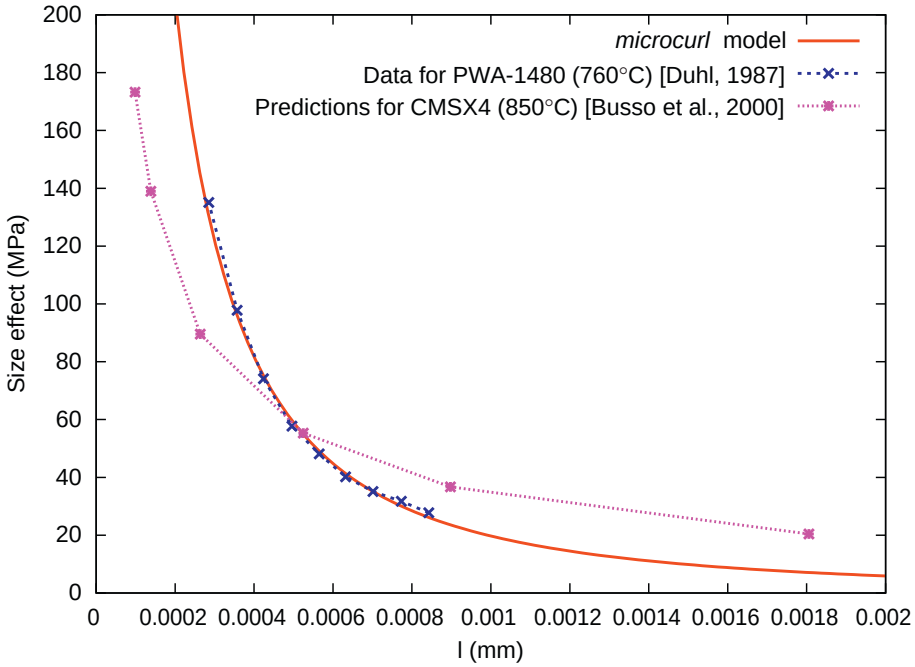

Fig. 13. Comparison between experimental data, in the form of precipitate size vs. size effect strengthening (extra-stress above the size-independent value) published for a two-phase material (γ matrix phase elasto-viscoplastic and quasi-elastic γ' precipitates) from Duhl (1987), the prediction of Busso et al. (2000) and that obtained using the *microcurl* model. The volume fraction of precipitates is f_h=68%, critical resolved shear stress of the matrix phase $\tau_c = 59\,\text{MPa}, \mu = 100\,000\,\text{MPa}, H^h_\chi = H^s_\chi = 7\times10^5\,\text{MPa}$, A^h=$3.5\times10^{-6}\,\text{MPa mm}^2$ and A^s=$4\times10^{-5}\,\text{MPa mm}^2$.

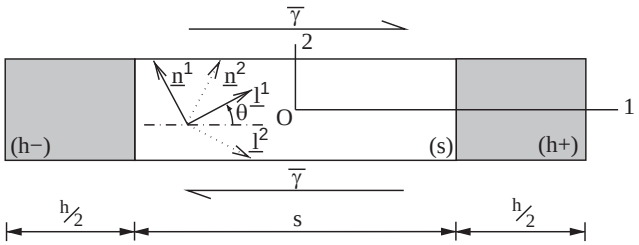

Fig. 14. Double slip in a two-phase periodic laminate microstructure under simple shear.

The plastic micro-deformation tensor takes the same form as that in Section 4.4. However, in contrast to the case of single slip, we expect the component χ^p_{21} of the plastic micro-deformation not to vanish. The matrix expressions (106) are still valid in the double slip context. In particular, there is still one single non-zero component in the curl of plastic micro-deformation. The resulting stress tensors are

$$[\underset{\sim}{\boldsymbol{\sigma}}] = \mu \begin{bmatrix} 0 & \overline{\gamma} - H^p_{12} - H^p_{21} + u_{2,1} & 0 \\ \overline{\gamma} - H^p_{12} - H^p_{21} + u_{2,1} & 0 & 0 \\ 0 & 0 & 0 \end{bmatrix}, \tag{152}$$

$$[\underset{\sim}{\boldsymbol{s}}] = -H_\chi \begin{bmatrix} 0 & H^p_{12} - \chi^p_{12} & 0 \\ H^p_{21} - \chi^p_{21} & 0 & 0 \\ 0 & 0 & 0 \end{bmatrix}, \tag{153}$$

$$[\underset{\sim}{\boldsymbol{M}}] = \begin{bmatrix} 0 & 0 & -A\chi^p_{12,1} \\ 0 & 0 & 0 \\ 0 & 0 & 0 \end{bmatrix}, \quad [\operatorname{curl} \underset{\sim}{\boldsymbol{M}}] = \begin{bmatrix} 0 & -A\chi^p_{12,11} & 0 \\ 0 & 0 & 0 \\ 0 & 0 & 0 \end{bmatrix}. \tag{154}$$

Consequently, the double stress has only one non-vanishing component related to χ^p_{12} as in the case of single slip. Therefore the balance equation, $\underset{\sim}{\boldsymbol{s}} = -\operatorname{curl} \underset{\sim}{\boldsymbol{M}}$, becomes

$$\begin{cases} -H_\chi (H^p_{12} - \chi^p_{12}) = A\chi^p_{12,11}, \\ H^p_{21} - \chi^p_{21} = 0. \end{cases} \tag{155}$$

It is also found that the component χ_{21}^p does not contribute to the dislocation density tensor. It is bound to coincide with the plastic deformation H_{21}^p, according to the second balance equation. This will be due to the fact that no contribution of the component χ_{21}^p will appear in the back stress, as it is shown by the plasticity criterion $|\underset{\sim}{\boldsymbol{\sigma}} : \underset{\sim}{\boldsymbol{P}}^{\alpha} + \underset{\sim}{\boldsymbol{s}} : \underset{\sim}{\boldsymbol{P}}^{\alpha}| = \tau_c$:

$$|\sigma_{12}(\cos^2\theta - \sin^2\theta) + s_{12}\cos^2\theta| = |\sigma_{12}(\cos^2\theta - \sin^2\theta) + A\chi_{12,11}^p \cos^2\theta| = \tau_c. \tag{156}$$

In the same way as for the single slip case, the profile of χ_{12}^p is parabolic in the plastic phase. It is computed as in Eq. (112), which involves integration constants that can be identified as in Section 4.4 based on interface conditions. The resulting plastic slip is

$$\gamma = \frac{1}{2\cos^2\theta}\left(\chi_{12}^{ps} - \frac{A^s}{H_\chi^s}\chi_{12,11}^{ps}\right). \tag{157}$$

Since we have $\chi_{21}^{ps} = -2\gamma\sin^2\theta$, the profile of χ_{21}^p is parabolic in the plastic phase as well. In the elastic phase, the balance equations (155) are still valid with vanishing plastic slip. Then, one obtains

$$\begin{cases} \chi_{12}^{ph} = \dfrac{A^h}{H_\chi^h}\chi_{12,11}^p, \\ \chi_{21}^{ph} = 0. \end{cases} \tag{158}$$

Therefore, the component χ_{12}^p has a hyperbolic profile in the hard phase and can be computed as in Eq. (113); and its profile over the whole structure is similar to the single slip case. In addition, the component χ_{21}^p vanishes in the elastic domain and it cannot be continuous at the interface as soon as $\gamma \neq 0$. Accordingly, the *microcurl* model only ensures the continuity of the component χ_{12}^p, which contributes to the dislocation density tensor. Here the complete analytical solution with χ_{21}^p discontinuous at the interface between the two phases has been obtained. The expressions of the integration constants as functions of $\overline{\gamma}$ are

$$a^s = \frac{\frac{\tau_c}{\cos^2\theta - \sin^2\theta} - \overline{\gamma}}{(1-\tan^2\theta)\left(\frac{l^2 f_s^3}{6} + \frac{l f_s^2 A^s \coth(\omega^h h/2)}{A^h\omega^h} + \frac{2f_s A^s}{H_\chi^s} + \frac{2f_s A^s}{\mu(1-\tan^2\theta)^2}\right)}, \tag{159}$$

$$a^h = -\frac{a^s A^s s}{A^h\omega^h \sinh\left(\frac{\omega^h h}{2}\right)}, \tag{160}$$

$$c = -a^s\left(\frac{s^2}{4} + \frac{A^s \coth\left(\frac{\omega^h h}{2}\right)}{A^h\omega^h}\right). \tag{161}$$

Fig. 15 illustrates the continuity of χ_{12}^p and the discontinuity of χ_{21}^p at the interface. The problem of interface conditions in strain gradient plasticity has already been pointed out, for example in Aifantis and Willis (2005) and Gurtin and Needleman (2005). In these publications, jump conditions at interfaces are discussed. Here, no jump condition is imposed on χ_{21}^p at the interface, instead, continuity requirements for χ_{12}^p and the double traction tensor are enforced. In order to illustrate the size effects obtained with double symmetric slip, the integration constant a^s has been obtained as a function of $\langle H_{12}^p \rangle$. It materialises that we find the same expression than in single slip, a^s being still given by Eq. (133). The Cosserat model also gives the same expression for a^s as a function of $\langle H_{12}^p \rangle$. The macroscopic stress Σ_{12} can be expressed by

$$\Sigma_{12} = \frac{\tau_c}{\cos^2\theta - \sin^2\theta} - \frac{2A^s a^s}{1-\tan^2\theta}. \tag{162}$$

Fig. 16 presents the predicted size effects in double symmetric slip for angles θ ranging from 0° to 90°. For the particular case of $\theta = 45^\circ$, no plastic slip is activated since the Schmid factors vanish. Note also that for the specific case of $\theta = 90^\circ$, no hardening effect is found. Indeed, in that situation, one single effective slip system is obtained. Under shear, one slip band forms parallel to the interface for a vanishing dislocation density tensor, that is $\underset{\sim}{\mathrm{curl}}\,\boldsymbol{H}^p = 0$. It can therefore be concluded that the generalised crystal plasticity models based on the dislocation density tensor do not regularise this strain localisation problem.

In order to sum up the influence of θ on size effects, the maximal size effect predicted by the models is calculated. For large microstructural length scales compared to the characteristic length, the macroscopic stress becomes

$$\lim_{l\to\infty}\Sigma_{12} = \frac{\tau_c}{\cos^2\theta - \sin^2\theta}, \tag{163}$$

as in classical crystal plasticity. On the other hand, for small microstructural length scales,

$$\lim_{l\to 0}\Sigma_{12} = \frac{\tau_c}{\cos^2\theta - \sin^2\theta} + \frac{1-f_s}{f_s}\frac{1}{1-\tan^2\theta}H_\chi\langle\gamma\rangle. \tag{164}$$

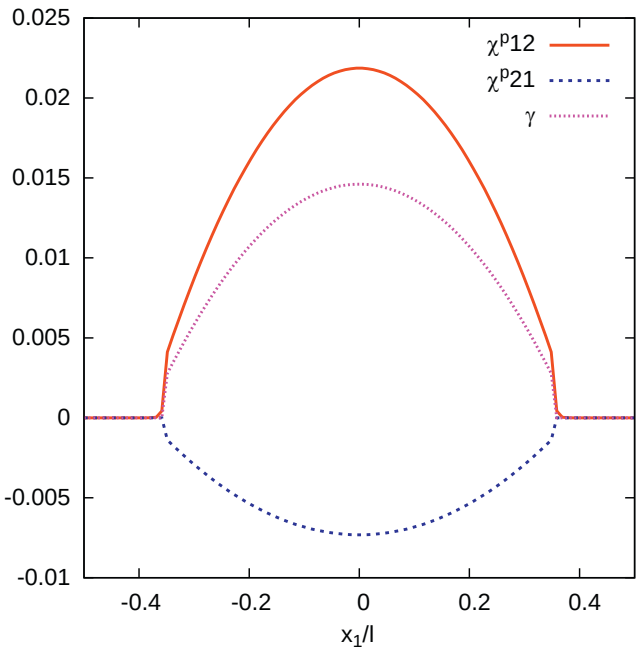

Fig. 15. Profiles of plastic micro-deformation χ^p_{12} and χ^p_{21} and of the plastic slip γ in the two-phase microstructure with the *microcurl* model, for symmetric double slip with $\theta=30^\circ$. The material parameters used in this case are: $\mu=35\,000$ MPa, $H^h_\chi=H^s_\chi=133\,829$ MPa, $A^h=2\times10^{-6}$ MPa mm^2, A^s=2×10^{-5} MPa mm^2 and $\tau_c=40$ MPa. f_s=0.7 and the values of $\beta^{h,s}$ are chosen for $l=1$ μm. This figure shows that in the case of double slip, χ^p_{12} is continuous at the interface while χ^p_{21} is discontinuous.

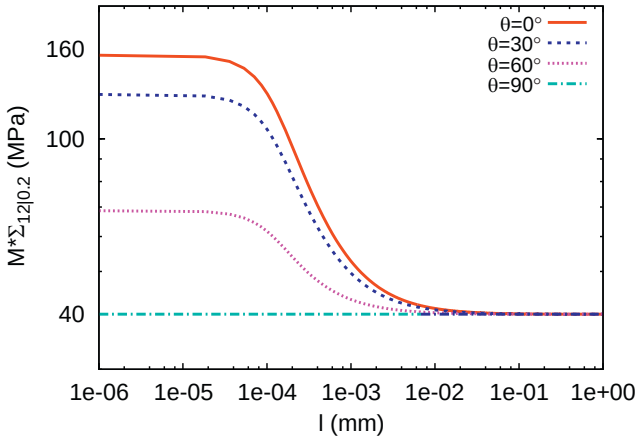

Fig. 16. Evolution of the macroscopic flow stress $\Sigma_{12|0.2}$ multiplied by the Schmid factor $M=\cos^2\theta-\sin^2\theta$ at $\langle H^p_{12}\rangle=0.002$ as a function of θ. The material parameters considered for each phase are given in Table 3.

Consequently, the maximal extra-stress reads

$$\Delta\Sigma=\frac{1-f_s}{f_s}\frac{1}{1-\tan^2\theta}H_\chi\langle\gamma\rangle. \tag{165}$$

The maximal size effect as a function of θ predicted by the models is presented in Fig. 17.

7. Conclusions

The main results obtained in this work can be summarised as follows:

1. A micromorphic crystal plasticity model, called *microcurl*, has been proposed to regularise the response of a strain gradient plasticity model in the presence of an elastic phase. The "*curl* H^p" model is retrieved when the coupling modulus H_χ that arises in the *microcurl* model, becomes a Lagrange multiplier. The corresponding internal constraint states that the plastic micro-deformation $\boldsymbol{\chi}^p$ coincides with conventional plastic deformation $\boldsymbol{H}^p$.
2. A complete solution of stress, strain and plastic slip distributions could be worked out for a two-phase laminate microstructure where the behaviour of the elastic and elasto-plastic phases are described by the Cosserat or *microcurl*

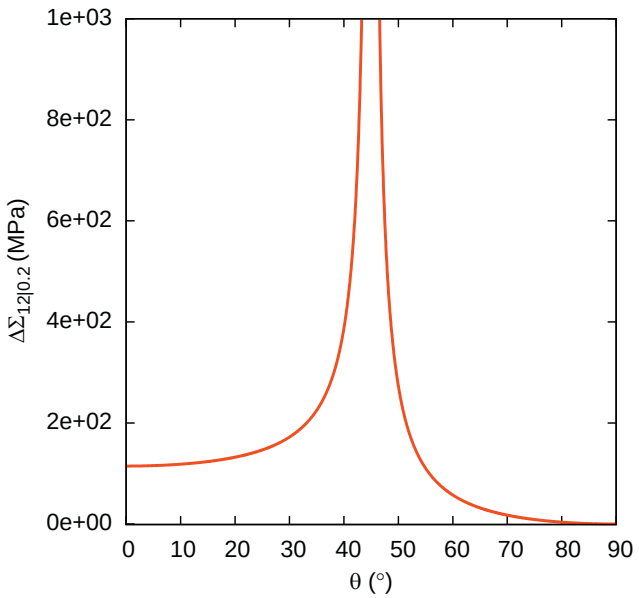

Fig. 17. Evolution of the macroscopic yield stress $\Delta\Sigma_{12|0.2}$ as a function of θ. The material parameters considered for each phase are given in Table 3.

model. In contrast, a discontinuity remains with the "*curl* H^p" model due to the question of transmission of higher order tractions from the plastic to the elastic phase. It was also found that the Cosserat and *microcurl* solutions coincide for a certain range of values of material parameters.

3. The size effect in terms of extra-hardening amplitude, predicted by the Cosserat model is bounded. In contrast, this amplitude is linearly related to the coupling modulus H_χ in the *microcurl* model. Accordingly, the *microcurl* model can accommodate any observed amplitude of extra-hardening.
4. A size-dependent transition domain between two asymptotic regimes has been detected for both models, for small and large microstructural length scales respectively. The location of this transition domain, defined by l_c, has been determined and can be calibrated to comply with experimental results observed either at the nano or micron scales. This characteristic length is mainly controlled by the parameter A^s and A^h.
5. The power law exponents for the scaling laws were determined, ranging from $n=0$ to -2. It comprises therefore the ideal Orowan and Hall-Petch exponents. The higher order parameters A and H_χ can be calibrated to match experimental results in a given domain of length scales. More specifically, the *microcurl* model can produce scaling laws between 0 and -2. The Cosserat model produces scaling laws from 0 to -1 depending on the volume fraction of the soft phase. In contrast, the "*curl* H^p" model invariably leads to an asymptotic regime with $n=-2$.
6. The formulation of the three models considered in this work is such that a back stress component arises in the soft phase and macroscopically results in linear kinematic hardening. The corresponding kinematic hardening modulus was explicitly derived as a function of higher order material parameters, volume fraction of soft phase, and microstructural length scale. It is bounded in the case of the Cosserat model, whereas it is linearly related to H_χ according to the *microcurl* model.
7. The models are applicable to multislip conditions. The analysis in the case of symmetric double slip has revealed a similar size-dependent behaviour as in single slip, and the existence of a possible discontinuity of some plastic micro-deformation components.

In the three model formulations presented in this work, the double stress tensor belongs to the arguments of the free energy function only, and not of the dissipation potential. This simple framework is sufficient to illustrate the existence of a back stress and to work out explicit analytic results for the laminate problem. However, dissipative mechanisms related to generalised stresses can be introduced in a systematic manner following the work of Forest and Sievert (2003), Forest (2009) and Gurtin and Anand (2009). The theory can also be formulated assuming finite deformation kinematics following the framework proposed in Forest and Sievert (2003) for micromorphic continua. This formulation is based on the usual multiplicative decomposition of the deformation gradient into elastic and plastic parts. Such decompositions exist also for the micro-deformation and its gradient. However, in the present single crystal model, there will be no need for decomposing $\underset{\sim}{\boldsymbol{\chi}}^p$ and $\underset{\sim}{\boldsymbol{\Gamma}}_\chi$ as long as no additional dissipative mechanisms are introduced. The internal constraint corresponding to Eq. (103) would then be $\underset{\sim}{\boldsymbol{\chi}}^p \equiv \underset{\sim}{\boldsymbol{F}}^p - \underset{\sim}{\mathbf{1}}$ where $\underset{\sim}{\boldsymbol{F}}^p$ is the plastic deformation in the multiplicative decomposition.

The proposed models should now be applied to more realistic cases, for example to predict size effects in Ni-base superalloys or in polycrystals based on large scale finite element simulations, as done in Forest et al. (2000). The fact that

the Cosserat extra-hardening stress was found to be bounded, irrespective of the value of higher order moduli, may explain that the grain size effects for aggregates of Cosserat crystals are systematically underestimated in Forest et al. (2000) and Zeghadi et al. (2005). It is expected that predicted size-effects will be more pronounced for the *microcurl* model that with the Cosserat model.

The linear kinematic hardening predicted by the models in the laminate microstructure is quite ideal and unrealistic. A dependence of the linear kinematic hardening on total dislocation density was shown in Groma et al. (2003) and Forest (2008). More generally, the constitutive framework should be extended to include non-linear kinematic hardening.

From the numerical point of view, the Cosserat model has the advantage that it requires only three additional degrees of freedom compared to the nine generally required in the "*curl* H^p" and *microcurl* models. Models involving the slips γ^α themselves or the dislocation densities as additional degrees of freedom, like that of Bayley et al. (2006), are even more expensive since the number of degrees of freedom increases proportionally to the number of slip systems. The possible discontinuity of some components of the plastic micro-deformation makes the finite element implementation of the *microcurl* model quite complex.

Under single slip conditions, the models discussed here have a sound physical basis as shown by comparison with theoretical results using statistical dislocation concepts and also simple line tension dislocation models (e.g., see Forest, 2008). In contrast, the application of the models to multislip conditions is possible in a purely phenomenological way, by identifying the material parameters from experimental data, or from comparison with dislocation dynamics simulations. This remains to be done with a view to highlight the limitations of the approach.

Interface conditions with simple continuity requirements have played a major role in the present work. However, enriched interface conditions and constitutive equations at grain boundaries, as proposed in Aifantis and Willis (2005) and Gurtin and Anand (2008), could be more realistic. Some aspects of such interface laws should even be identified from atomistic simulations (see, for instance, McDowell, 2008).

Acknowledgements

One part of this work was performed within the NANOCRYSTAL project ANR-07-BLAN-0186. Financial support of ANR is gratefully acknowledged.

Appendix A. Notations

First-rank, second-rank and fourth-rank tensors are respectively denoted by $\underline{\boldsymbol{A}}$, $\underset{\sim}{\boldsymbol{A}}$ and $\underset{\approx}{\boldsymbol{A}}$. The superscripts $\underset{\sim}{\boldsymbol{A}}^s$ and $\underset{\sim}{\boldsymbol{A}}^a$ will denote respectively the symmetric and skew-symmetric parts of the tensor. Both intrinsic and index notations are given at some places for clarity.

The intrinsic definition of the curl operator applied to a tensor T of any rank in any coordinate system q^i is

$$\mathrm{curl}\, T = \frac{\partial T}{\partial q^i} \times \underline{\boldsymbol{e}}^i, \tag{166}$$

where $\times$ denotes the vector product. In a Cartesian frame and for a tensor of rank two, this gives

$$\mathrm{curl}\, \underset{\sim}{\boldsymbol{A}} = \frac{\partial \underset{\sim}{\boldsymbol{A}}}{\partial x_l} \times \underline{\boldsymbol{e}}_l = A_{ik,l}\underline{\boldsymbol{e}}_i \otimes (\underline{\boldsymbol{e}}_k \times \underline{\boldsymbol{e}}_l) = \epsilon_{jkl} A_{ik,l}\underline{\boldsymbol{e}}_i \otimes \underline{\boldsymbol{e}}_j, \tag{167}$$

where ϵ_{ijk} is the permutation tensor. Hence

$$(\mathrm{curl}\, \underset{\sim}{\boldsymbol{A}})_{ij} = \epsilon_{jkl} A_{ik,l}. \tag{168}$$

Note that the definition of the curl operator chosen in Cermelli and Gurtin (2001) is the *opposite and transpose* of (168).

Finally, brackets $\langle\ \rangle$ are used to compute average values over a unit cell V:

$$\langle - \rangle = \frac{1}{V}\int_V - dV. \tag{169}$$

Appendix B. Strain gradient plasticity solution for a two-phase plastic laminate

A complete solution of the laminate boundary value problem can be derived for the two-phase periodic microstructure under simple shear for the "*curl* H^p" model of Section 3 when both phases exhibit a plastic behaviour. The hard phase now admits a critical resolved shear stress τ_c^h. In both phases, under plastic loading conditions, the plastic slip has a parabolic profile:

$$\gamma^h(x_1) = a^h x_1^2 + b^h x_1 + c^h, \quad \gamma^s(x_1) = a^s x_1^2 + b^s x_1 + c^s \tag{170}$$

taken over the interval $[-s/2,s/2+h]$, with six coefficients to be determined from the following conditions:

- Continuity of plastic slip at $x_1 = s/2$ and periodicity of plastic slip at $x_1 = -s/2$ and $x_1 = s/2+h$:

$$a^s\left(\frac{s}{2}\right)^2+b^s\frac{s}{2}+c^s=a^h\left(\frac{s}{2}\right)^2+b^h\frac{s}{2}+c^h, \tag{171}$$

$$a^s\left(\frac{s}{2}\right)^2-b^s\frac{s}{2}+c^s=a^h\left(\frac{s}{2}+h\right)^2+b^h\left(\frac{s}{2}+h\right)+c^h. \tag{172}$$

- Continuity of double stress component $M_{13}=-A\gamma_{,1}$ at $x_1 = s/2$ and periodicity of double stress vector at $x_1=-s/2$ and $s/2+h$:

$$A^s\left(2a^s\frac{s}{2}+b^s\right)=A^h\left(2a^h\frac{s}{2}+b^h\right), \tag{173}$$

$$A^s\left(-2a^s\frac{s}{2}+b^s\right)=A^h\left(2a^h\left(\frac{s}{2}+h\right)+b^h\right). \tag{174}$$

- Plasticity criterion

$$\sigma_{12}+2A_sa^s=\tau_c^s, \tag{175}$$

$$\sigma_{12}+2A_ha^h=\tau_c^h. \tag{176}$$

- Symmetry condition at $x_1 = 0$:

$$\gamma_{,1}(0)=0. \tag{177}$$

- Periodicity condition for the perturbation u_2 translated into the following terms. The elastic law provides

$$u_{2,1}=\sigma_{12}/\mu-\overline{\gamma}+\gamma. \tag{178}$$

The mean value over one unit cell of the left-hand side necessarily vanishes since u_2 is periodic:

$$(s+h)\langle u_{2,1}\rangle=(s+h)\langle\sigma_{12}/\mu-\overline{\gamma}+\gamma\rangle=\int_{-s/2}^{s/2}(\tau_c^s/\mu-2A^sa^s/\mu-\overline{\gamma}+a^sx_1^2+c^s)\,dx_1+\int_{s/2}^{s/2+h}(\tau_c^h/\mu-2A^ha^h/\mu-\overline{\gamma}+a^hx_1^2+c^h)\,dx_1$$
$$=(\tau_c^s/\mu-2A^sa^s/\mu-\overline{\gamma})(s+h)+sc^s+hc^h+\frac{2a^s}{3}\left(\frac{s}{2}\right)^3+\frac{2a^h}{3}\left(\left(\frac{s}{2}+h\right)^3-\left(\frac{s}{2}\right)^3\right)+\frac{b^h}{2}\left(\left(\frac{s}{2}+h\right)^2-\left(\frac{s}{2}\right)^2+h(s+h)\right).$$

From Eq. (177) we obtain

$$b^s=0. \tag{179}$$

The combination (175)–(176) provides the relation

$$2(A^sa^s-A^ha^h)=\tau_c^s-\tau_c^h. \tag{180}$$

From the combination of Eqs. (173) and (180), one finds

$$b^h=\frac{\tau_c^s-\tau_c^h}{A^h}\frac{s}{2}. \tag{181}$$

The combination (171)–(172) yields

$$a^h=\frac{b^h}{s+h}=\frac{\tau_c^s-\tau_c^h}{A^h}\frac{s}{2(s+h)}. \tag{182}$$

Finally,

$$a^s=\frac{\tau_c^s-\tau_c^h}{A^s}\frac{2s+h}{2(s+h)}. \tag{183}$$

Eqs. (171) (or (172)) and (179) provide a system of two equations from which we obtain c^h and c^s.

Appendix C. Double traction at the interface

The purpose of this appendix is to propose a way to derive, from the microcurl model, the jump of generalized tractions presented in Section 3. It was shown that with the "*curl* H^p" model, the required continuity of the double traction tensor, $\underset{\sim}{\boldsymbol{m}}$, see Eq. (58), leads to a physically not relevant solution of the boundary value problem. So, the correct value of the double traction to be imposed at the interface was left undetermined. This value can be obtained as the limiting case of the *microcurl* model for which we have solved the full boundary value problem. As we want the *microcurl* model to tend to the "*curl* H^p" model, we have to consider an infinite coupling modulus, $H_\chi\to\infty$. In that case, χ_{12}^{ps} is equal to the plastic

slip γ and then we have

$$\lim_{H_\chi \to \infty} \chi_{12}^{ps}(\pm s/2) = 0, \tag{184}$$

which means that the plastic micro-deformation tends to zero at the interfaces with the elastic phase.

We evaluate the double traction tensor at the interfaces:

$$\lim_{H_\chi \to \infty} m_{12}(\pm s/2) = \lim_{H_\chi \to \infty} A^s \chi_{12,1}^{ps}(\pm s/2) = -\frac{A^s \mathcal{A} f_s l}{\mathcal{B} l^2 + \frac{2A^s}{\mu}} = \frac{A^s \left(\overline{\gamma} - \frac{\tau_c}{\mu}\right) f_s l}{\frac{f_s^3}{6} l^2 + \frac{2A^s}{\mu}}. \tag{185}$$

This expression can be transformed into the following expression:

$$\lim_{H_\chi \to \infty} m_{12}(\pm s/2) = -\frac{A^s \mathcal{A}' f_s}{\mathcal{B}' l} = \frac{6A^s \langle \gamma \rangle}{f_s^2 l}. \tag{186}$$

Eqs. (185) and (186) give us the value of the double traction tensor at the interfaces in the limit case of the *microcurl* model. We can now return to the original "*curl* H^p" model and impose the appropriate value of the double traction (and double stress) component m_{12} (and M_{13}) at the interface. The corresponding boundary value problem is then well-posed and can be solved for the plastic deformation profile.

References

Acharya, A., Bassani, J.L., 2000. Lattice incompatibility and a gradient theory of crystal plasticity. Journal of the Mechanics and Physics of Solids 48, 1565–1595.

Acharya, A., Beaudoin, A.J., 2000. Grain size effects in viscoplastic polycrystals at moderate strains. Journal of the Mechanics and Physics of Solids 48, 2213–2230.

Aifantis, E.C., 1984. On the microstructural origin of certain inelastic models. Journal of Engineering Materials and Technology 106, 326–330.

Aifantis, E.C., 1987. The physics of plastic deformation. International Journal of Plasticity 3, 211–248.

Aifantis, K.E., Willis, J.R., 2005. The role of interfaces in enhancing the yield strength of composites and polycrystals. Journal of the Mechanics and Physics of Solids 53, 1047–1070.

Bammann, D.J., 2001. A model of crystal plasticity containing a natural length scale. Materials Science and Engineering A 309–310, 406–410.

Bardella, L., 2007. Some remarks on the strain gradient crystal plasticity modelling, with particular reference to the material length scales involved. International Journal of Plasticity 23, 296–322.

Bassani, J.L., 2001. Incompatibility and a simple gradient theory of plasticity. Journal of the Mechanics and Physics of Solids 49, 1983–1996.

Bayley, C.J., Brekelmans, W.A.M., Geers, M.G.D., 2006. A comparison of dislocation induced back stress formulations in strain gradient crystal plasticity. International Journal of Solids and Structures 43, 7268–7286.

Bittencourt, E., Needleman, A., Gurtin, M., Van der Giessen, E., 2003. A comparison of nonlocal continuum and discrete dislocation plasticity predictions. Journal of the Mechanics and Physics of Solids 51 (2), 281–310.

Busso, E.P., Meissonier, F.T., O'Dowd, N.P., 2000. Gradient-dependent deformation of two-phase single crystal. Journal of Mechanics and Physics of Solids 48 (11), 2333–2361.

Cermelli, P., Gurtin, M.E., 2001. On the characterization of geometrically necessary dislocations in finite plasticity. Journal of the Mechanics and Physics of Solids 49, 1539–1568.

Cheong, K.S., Busso, E.P., Arsenlis, A., 2005. A study of microstructural length scale effects on the behavior of FCC polycrystals using strain gradient concepts. International Journal of Plasticity 21, 1797–1814.

Clayton, J.D., McDowell, D.L., Bammann, D.J., 2006. Modeling dislocations and disclinations with finite micropolar elastoplasticity. International Journal of Plasticity 22, 210–256.

Duhl, D.N., 1987. Directionally solidified superalloys. In: Superalloys II—High Temperature Materials for Aerospace and Industrial Power. Wiley-Interscience, John Wiley and Sons, pp. 189–214.

Eringen, A.C., Claus, W.D., 1970. A micromorphic approach to dislocation theory and its relation to several existing theories. In: Simmons, J.A., de Wit, R., Bullough, R. (Eds.), Fundamental Aspects of Dislocation Theory. National Bureau of Standards (US) Special Publication 317, II, pp. 1023–1062.

Fleck, N.A., Hutchinson, J.W., 1997. Strain gradient plasticity. Advances in Applied Mechanics 33, 295–361.

Forest, S., 2008. Some links between cosserat, strain gradient crystal plasticity and the statistical theory of dislocations. Philosophical Magazine 88, 3549–3563.

Forest, S., 2009. The micromorphic approach for gradient elasticity, viscoplasticity and damage. ASCE Journal of Engineering Mechanics 135, 117–131.

Forest, S., Barbe, F., Cailletaud, G., 2000. Cosserat modelling of size effects in the mechanical behaviour of polycrystals and multiphase materials. International Journal of Solids and Structures 37, 7105–7126.

Forest, S., Cailletaud, G., Sievert, R., 1997. A Cosserat theory for elastoviscoplastic single crystals at finite deformation. Archives of Mechanics 49 (4), 705–736.

Forest, S., Pradel, F., Sab, K., 2001. Asymptotic analysis of heterogeneous Cosserat media. International Journal of Solids and Structures 38, 4585–4608.

Forest, S., Sedláček, R., 2003. Plastic slip distribution in two-phase laminate microstructures: dislocation-based vs. generalized-continuum approaches. Philosophical Magazine A 83, 245–276.

Forest, S., Sievert, R., 2003. Elastoviscoplastic constitutive frameworks for generalized continua. Acta Mechanica 160, 71–111.

Ghoniem, N.M., Busso, E.P., Kioussis, N., Huang, H., 2003. Multiscale modelling of nanomechanics and micromechanics: an overview. Philosophical Magazine 83, 3475–3528.

Groma, I., Csikor, F.F., Zaiser, M., 2003. Spatial correlations and higher-order gradient terms in a continuum description of dislocation dynamics. Acta Materialia 51, 1271–1281.

Gurtin, M.E., 2002. A gradient theory of single-crystal viscoplasticity that accounts for geometrically necessary dislocations. Journal of the Mechanics and Physics of Solids 50, 5–32.

Gurtin, M.E., Anand, L., 2008. Nanocrystalline grain boundaries that slip and separate: a gradient theory that accounts for grain-boundary stress and conditions at a triple-junction. Journal of the Mechanics and Physics of Solids 56, 184–199.

Gurtin, M.E., Anand, L., 2009. Thermodynamics applied to gradient theories involving the accumulated plastic strain: the theories of Aifantis and Fleck & Hutchinson and their generalization. Journal of the Mechanics and Physics of Solids 57, 405–421.

Gurtin, M.E., Needleman, A., 2005. Boundary conditions in small-deformation single crystal plasticity that account for the Burgers vector. Journal of the Mechanics and Physics of Solids 53, 1–31.

Hunter, A., Koslowski, M., 2008. Direct calculations of material parameters for gradient plasticity. Journal of the Mechanics and Physics of Solids 56 (11), 3181–3190.
Kröner, E., 1963. On the physical reality of torque stresses in continuum mechanics. International Journal of Engineering Science 1, 261–278.
Lele, S.P., Anand, L., 2008. A small-deformation strain-gradient theory for isotropic viscoplastic materials. Philosophical Magazine 88, 3655–3689.
Liebe, T., Menzel, A., Steinmann, P., 2003. Theory and numerics of geometrically non-linear gradient plasticity. International Journal of Engineering Science 41, 1603–1629.
McDowell, D.L., 2008. Viscoplasticity of heterogeneous metallic materials. Materials Science and Engineering R 62, 67–123.
Nye, J.F., 1953. Some geometrical relations in dislocated crystals. Acta Metallurgica 1, 153–162.
Sedláček, R., Forest, S., 2000. Non-local plasticity at microscale: a dislocation-based model and a Cosserat model. Physica Status Solidi (b) 221, 583–596.
Shu, J.Y., 1998. Scale-dependent deformation of porous single crystals. International Journal of Plasticity 14, 1085–1107.
Shu, J.Y., Fleck, N.A., Van der Giessen, E., Needleman, A., 2001. Boundary layers in constrained plastic flow: comparison of non local and discrete dislocation plasticity. Journal of the Mechanics and Physics of Solids 49, 1361–1395.
Smyshlyaev, V.P., Fleck, N.A., 1996. The role of strain gradients in the grain size effect for polycrystals. Journal of the Mechanics and Physics of Solids 44, 465–495.
Steinmann, P., 1996. Views on multiplicative elastoplasticity and the continuum theory of dislocations. International Journal of Engineering Science 34, 1717–1735.
Svendsen, B., 2002. Continuum thermodynamic models for crystal plasticity including the effects of geometrically-necessary dislocations. Journal of the Mechanics and Physics of Solids 50, 1297–1329.
Tinga, T., Brekelmans, W.A.M., Geers, M.G.D., 2008. Incorporating strain gradient effects in a multiscale constitutive framework for nickel-base superalloys. Philosophical Magazine 88, 3793–3825.
Yefimov, S., Groma, I., Van der Giessen, E., 2004. A comparison of a statistical-mechanics based plasticity model with discrete dislocation plasticity calculations. Journal of the Mechanics and Physics of Solids 52, 279–300.
Yefimov, S., Van der Giessen, E., 2005. Multiple slip in a strain-gradient plasticity model motivated by a statistical-mechanics description of dislocations. International Journal of Solids and Structures 42, 3375–3394.
Zeghadi, A., Forest, S., Gourgues, A.-F., Bouaziz, O., 2005. Cosserat continuum modelling of grain size effects in metal polycrystals. Proceedings in Applied Mathematics and Mechanics 5, 79–82.